Circulation Research
JOURNAL OF THE AMERICAN HEART ASSOCIATION

Magnetic Targeting Enhances Engraftment and Functional Benefit of Iron-Labeled Cardiosphere-Derived Cells in Myocardial Infarction

Ke Cheng, Tao-Sheng Li, Konstantinos Malliaras, Darryl R. Davis, Yiqiang Zhang and Eduardo Marbán

Circ. Res. 2010;106;1570-1581; originally published online Apr 8, 2010;
DOI: 10.1161/CIRCRESAHA.109.212589
Circulation Research is published by the American Heart Association. 7272 Greenville Avenue, Dallas, TX 72514
 Print ISSN: 0009-7330. Online ISSN: 1524-4571

Magnetic Targeting Enhances Engraftment and Functional Benefit of Iron-Labeled Cardiosphere-Derived Cells in Myocardial Infarction

Ke Cheng, Tao-Sheng Li, Konstantinos Malliaras, Darryl R. Davis, Yiqiang Zhang, Eduardo Marbán

Rationale: The success of cardiac stem cell therapies is limited by low cell retention, due at least in part to washout via coronary veins.

Objective: We sought to counter the efflux of transplanted cells by rendering them magnetically responsive and imposing an external magnetic field on the heart during and immediately after injection.

Methods and Results: Cardiosphere-derived cells (CDCs) were labeled with superparamagnetic microspheres (SPMs). In vitro studies revealed that cell viability and function were minimally affected by SPM labeling. SPM-labeled rat CDCs were injected intramyocardially, with and without a superimposed magnet. With magnetic targeting, cells were visibly attracted toward the magnet and accumulated around the ischemic zone. In contrast, the majority of nontargeted cells washed out immediately after injection. Fluorescence imaging revealed more retention of transplanted cells in the heart, and less migration into other organs, in the magnetically targeted group. Quantitative PCR confirmed that magnetic targeting enhanced cell retention (at 24 hours) and engraftment (at 3 weeks) in the recipient hearts by ≈3-fold compared to nontargeted cells. Morphometric analysis revealed maximal attenuation of left ventricular remodeling, and echocardiography showed the greatest functional improvement, in the magnetic targeting group. Histologically, more engrafted cells were evident with magnetic targeting, but there was no incremental inflammation.

Conclusions: Magnetic targeting enhances cell retention, engraftment and functional benefit. This novel method to improve cell therapy outcomes offers the potential for rapid translation into clinical applications. (*Circ Res*. 2010;106:1570-1581.)

Key Words: cardiac progenitor cells ■ cell transplantation ■ myocardial infarction ■ targeted cell delivery

Stem cell transplantation is a promising therapeutic strategy for acute or chronic ischemic cardiomyopathy.[1] Low cell retention and engraftment are major obstacles to achieving a significant functional benefit irrespective of the cell type or model used.[2,3] Acute (≤24-hour) cell retention is normally less than 10%, regardless of the delivery route.[3] Initial studies highlighted apoptosis as the culprit underlying low engraftment,[4,5] but recent work has shown that venous drainage and the contraction of a beating heart account for significant loss of transplanted cells.[6,7] As short-term cell retention is a prerequisite for long-term cell engraftment and functional improvement, translatable methods to attenuate cell loss are highly desirable. Magnetic targeting represents a noninvasive approach to coax therapeutic agents (eg, drugs, cells) into desired regions.[8] In the cardiovascular arena, previous work has concentrated on endothelial cell-related therapies, using magnetic targeting to improve cell homing to grafts or stents.[9–14] Moreover, previous studies have evaluated only short-term cell retention, not long-term engraftment or functional benefits.[9–14]

Here, we examine myocardial rather than endothelial targeting, and quantify long-term cardiac engraftment and function after intramyocardial injection of iron-labeled cardiosphere-derived cells (CDCs) subjected to an external magnetic attractor.

Methods

An expanded Methods section is available in the Online Data Supplement at http://circres.ahajournals.org.

CDC Culture and Superparamagnetic Microsphere Labeling

CDCs were cultured from tissue samples of hearts explanted from 8-week-old male Wistar Kyoto (WKY) rats, as previously described.[15–17] CDCs were labeled with fluorescent (dragon green or flash red) superparamagnetic microsphere (SPM) particles (0.9 μm diameter; Bangs Laboratories) by coincubation in culture for 24 hours. Loading of SPMs into CDCs was confirmed by Prussian Blue staining[18] and dragon green fluorescence. Labeling efficiency was assessed by flow cytometry.

Original received November 23, 2009; revision received March 15, 2010; accepted March 26, 2010.

From the Heart Institute, Cedars-Sinai Medical Center, Los Angeles, Calif.

Correspondence to Eduardo Marbán, MD, PhD, The Heart Institute, Cedars-Sinai Medical Center, 8700 Beverly Blvd, 1090 Davis Building, Los Angeles, CA 90048. E-mail Eduardo.Marban@csmc.edu

Circulation Research is available at http://circres.ahajournals.org DOI: 10.1161/CIRCRESAHA.109.212589

Effects of SPM Labeling on CDC Properties

In vitro toxicity experiments were performed 24 hours after SPM labeling. Cell viability was assessed by Trypan Blue exclusion. Apoptosis and necrosis were assessed by flow cytometry (7AAD and Annexin-V stain).[15] Methods used to assess cell proliferation and attachment are described in Detailed Methods. Percentages of cells that expressed the antigens c-kit, CD31, CD34 and CD90 were assessed by flow cytometry.[15] The apoptotic/necrotic effects of SPM labeling were examined by TUNEL staining.[19] H_2O_2-treated cells and nontreated cells were routinely included as positive and negative controls, respectively. Reactive oxygen species generation was measured by 2 commercially available kits following manufacturers' protocols.

In Vitro Cell Capture Experiments

SPM-labeled CDCs (500:1 SPM:cell ratio) were resuspended in PBS (1 million cells/mL) in a 15 mL conical tube. A 1.3 Tesla magnet was applied directly to the outside tube wall or 1 cm away from the tube for 20 seconds. Cell condensation was assessed visually. To better simulate the contracting and turbulent environment of myocardium, the same magnet was mounted on the outside wall of a cell suspension tube which was rotated at 60 RPM. After 24 hours, cell condensation by magnetic capturing was visually examined.

Cell Injection and Magnetic Targeting

Animal care was in accordance to Institutional Animal Care and Use Committee guidelines. Female WKY (n=88 total) rats underwent left thoracotomy under general anesthesia, and myocardial infarction (MI) was produced by permanent ligation of the left anterior descending coronary artery. The animals were subjected to intramyocardial injections with a 29-gauge needle at 4 points in the infarct border zone, with one of the following randomly assigned conditions: (1) Fe-CDC+magnet group: injection of 1 million SPM-labeled cells in 100 μL of PBS with a 1.3 Tesla magnet applied above the apex during the injection and for 10 minutes after injection; (2) Fe-CDC group: injection of 1 million SPM-labeled cells in 100 μL of PBS without magnet application; (3) CDC group: injection of 1 million nonlabeled cells in 100 μL of PBS with magnet applied above the apex during the injection and for another 10 minutes after injection; and (4) control group: injection of 100 μL of PBS without cells. A SPM control group was subsequently added: injection of 5×10^8 SPM beads (no cells) in 100 μL of PBS with magnet applied. A video recorder was attached to the surgical microscope to capture videos during cell injection.

Quantification of Engraftment by Real-Time PCR

Male CDCs were injected into female rats, enabling detection of the SRY gene (located on the Y chromosome) as an index of engraftment. Quantitative real-time PCR was performed 24 hours and 3 weeks after cell injection (n=6 for each cell-injected group).

Fluorescence Imaging

CDCs were labeled with SPMs that were conjugated with flash-red fluorophores (excitation: 660 nm; emission: 690 nm). Because of its long wavelength, flash-red is superior to dragon-green for imaging purposes. Hearts, lungs and spleens from representative animals from each group were harvested and imaged with the IVIS 200 (Xenogen) system to detect flash-red fluorescence. Hearts were washed with PBS to remove any cells adherent to the epicardium before imaging. Fluorescence signals (photon/s) from a fixed region of interest (ROI) were measured as described.[20]

Echocardiography

To assess global cardiac function in 53 rats (Fe-CDC+magnet [n=12], Fe-CDC [n=12], CDC [n=11], PBS control [n=9], and SPM control [n=9]), echocardiography was performed with the Vevo 770 system (Visual Sonics, Toronto, Canada) on day 0 post-MI and 3 weeks post-MI. The left ventricular ejection fraction (LVEF) was measured from the parasternal long-axis view. LVEF was calculated with Visual Sonics V1.3.8 software from 2D long-axis views taken through the infarcted area. Both absolute values and changes from baseline (day 0 post-MI) are reported.

Non-standard Abbreviations and Acronyms

α-SA	α-sarcomeric actin
CDC	cardiosphere-derived cell
FLI	fluorescence imaging
GFP	green fluorescent protein
LV	left ventricular
LVEF	left ventricular ejection fraction
MI	myocardial infarction
SPM	superparamagnetic microsphere
SPIO	superparamagnetic iron oxide
WKY	Wistar Kyoto

Morphometric and Histology Analysis

Subpopulations of CDCs from each group were virally transduced to express green fluorescent protein (GFP).[17] In these cases, flash-red-conjugated SPMs were used to avoid crossover with the fluorescence of GFP. Animals receiving GFP cells and flash-red SPMs were euthanized 3 weeks after injection. Hearts were cryo-sectioned and representative slides from each depth range were selected for immuohistochemistry. Quantitative morphometry analysis was performed as previously described.[21]

Statistical Analysis

Results are presented as means±SD unless specified otherwise. Statistical significance between baseline and 3 week LVEFs was determined using 2-tailed paired Student *t* test. All the other comparisons between any 2 groups were performed using 2-tailed unpaired Student *t* test. Comparison among more than 2 groups was analyzed by One-Way ANOVA followed by Bonferroni post hoc test. Differences were considered statistically significant when $P<0.05$.

Results

SPM Labeling Minimally Affects Cell Viability and Function

CDCs were labeled with Dragon-green fluorescence-conjugated SPM particles by coincubation in culture for 24 hours. Prussian Blue staining and fluorescence microscopy confirmed particle uptake by CDCs (Figure 1A and 1B). Nonlabeled cells did not exhibit Prussian Blue or Dragon-green fluorescence (insets, Figure 1A and 1B). These labeled cells are hereafter called SPM-labeled CDCs, or Fe-CDCs for short. Flow cytometry revealed an average labeling efficiency of 86.4±1.2% when a 500:1 SPM:cell ratio was used. The number of $TUNEL^+$ apoptotic cells increased with escalating SPM:cell ratio (red cells with white arrowheads, Figure 2A through 2C; Online Figure I). From the same images, it is also obvious that more SPMs (green color) were taken up by each cell at higher SPM dosages. Figure 2D and 2E shows typical Annexin/7-AAD flow cytometry plots. Further quantification (Figure 2F) indicated that SPM labeling induced <1% increase of apoptotic cells, but the SPM-labeled group had fewer necrotic cells. Given the fact that 500:1 labeling caused minimal cytotoxicity, this dosage was chosen for subsequent in vitro and in vivo experiments. Figure 2G through 2J shows

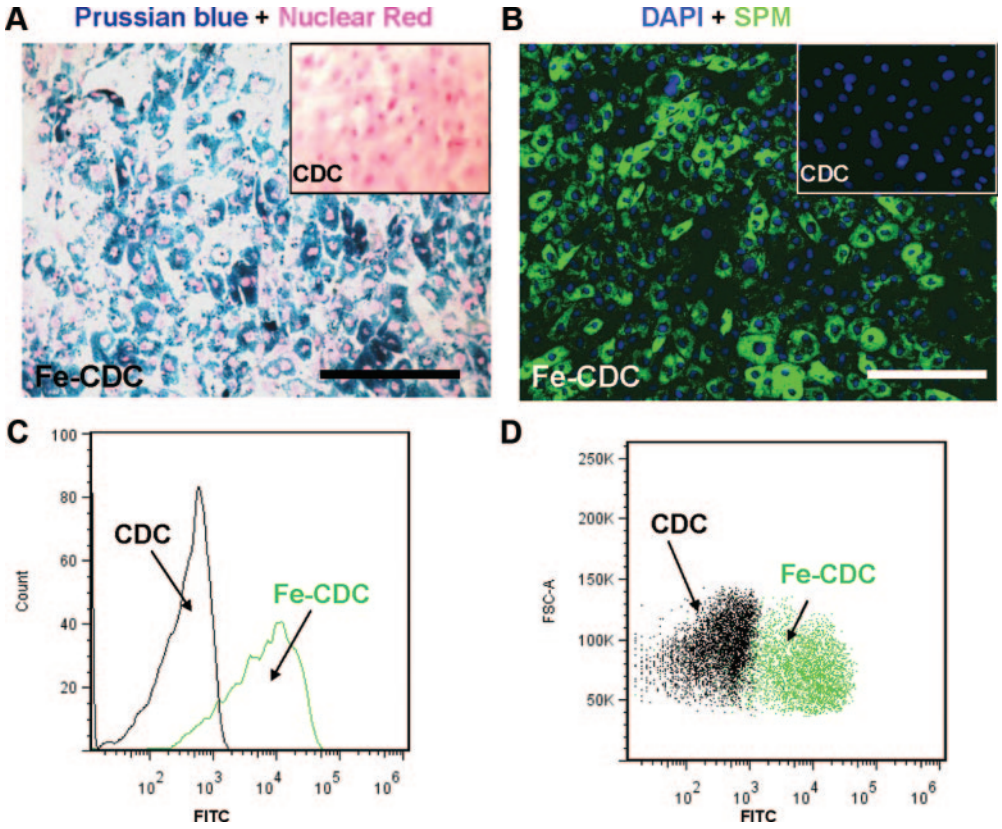

Figure 1. SPM labeling of CDCs. A, Rat CDCs were coincubated with SPMs for 24 hours at a 500:1 SPM:cell ratio. The cells were then fixed, stained for Prussian blue (iron), and counter-stained with nuclear red. **B,** CDCs were labeled with dragon-green–conjugated SPMs for 24 hours and then examined by fluorescence microscopy. Nonlabeled cells did not express Prussian blue or dragon-green fluorescence **(insets, A and B)**. **C and D,** Representative flow cytometric histogram and dot plots of SPM-labeled **(green)** and nonlabeled CDCs **(black)**. **Bars:** 100 μm in **A and B**.

that labeling with SPMs did not affect cell viability, proliferation, adhesion or antigenic phenotype of CDCs. In addition, SPM labeling did not lead to the generation of intracellular reactive oxygen species (Online Figure II).

External Magnet Captures SPM-Labeled CDCs In Vitro

To investigate the ability of a magnet to capture SPM-labeled CDCs in vitro, CDCs were loaded with 500:1 SPMs and resuspended in a conical tube (Online Figure III, A). After applying the magnet directly on the outer wall of the tube, CDCs were rapidly attracted toward the magnet and accumulated focally on the adjacent inner wall (Online Figure III, B). To gauge the effect of a more remote magnetic field, the magnet was moved 1 cm away from the tube and the capture experiment was repeated. SPM-labeled CDCs were still rapidly attracted toward the magnet and attached focally, albeit with smaller cell condensates (Online Figure III, C). To better mimic the myocardial environment, where turbulent flow exists, the same magnet was mounted on the outside of a rotating tube containing Fe-CDC suspension. Without the magnet, the cell suspension was uniform, with no focal condensation (Online Figure III, D). However, with the external magnet, Fe-CDCs formed a distinct condensate on the inner wall adjacent to the magnet (Online Figure III, E).

Magnetic Targeting Captures Fe-CDCs During Injection and Attenuates Washout Effect

One million CDCs derived from syngeneic male WKY rats were injected intramyocardially into the peri-infarct region of female hearts. White light imaging revealed that the majority of SPM-labeled CDCs (evident from their yellow-brown color) washed out within seconds (Online Movie I), diffusing from the injection site toward the base and then quickly disappearing. This confirms our prior conclusion[6] that initial washout accounts for significant cell loss. In contrast, Fe-CDCs injected with a magnet placed $\approx$1 cm above the cardiac apex moved toward the apex and accumulated around the infarct (Online Movie II). As seen in the movies, more cells are visible after injection in a heart from the Fe-CDC+magnet group (A) than in the Fe-CDC group (B). Thus, the external magnetic force was capable of effectively opposing the hydraulic forces that ordinarily drive washout.

Magnetic Targeting Improves Short-Term Retention and Long-Term Engraftment

Six animals from each cell-injected group were euthanized 24 hours after cell injection to assess short-term cell retention. Visual inspection of the excised hearts revealed that the Fe-CDC+magnet group (Figure 3B, red arrow) had more cells around the injection area than did the Fe-CDC group (Figure 3A). Likewise, representative fluorescence imaging

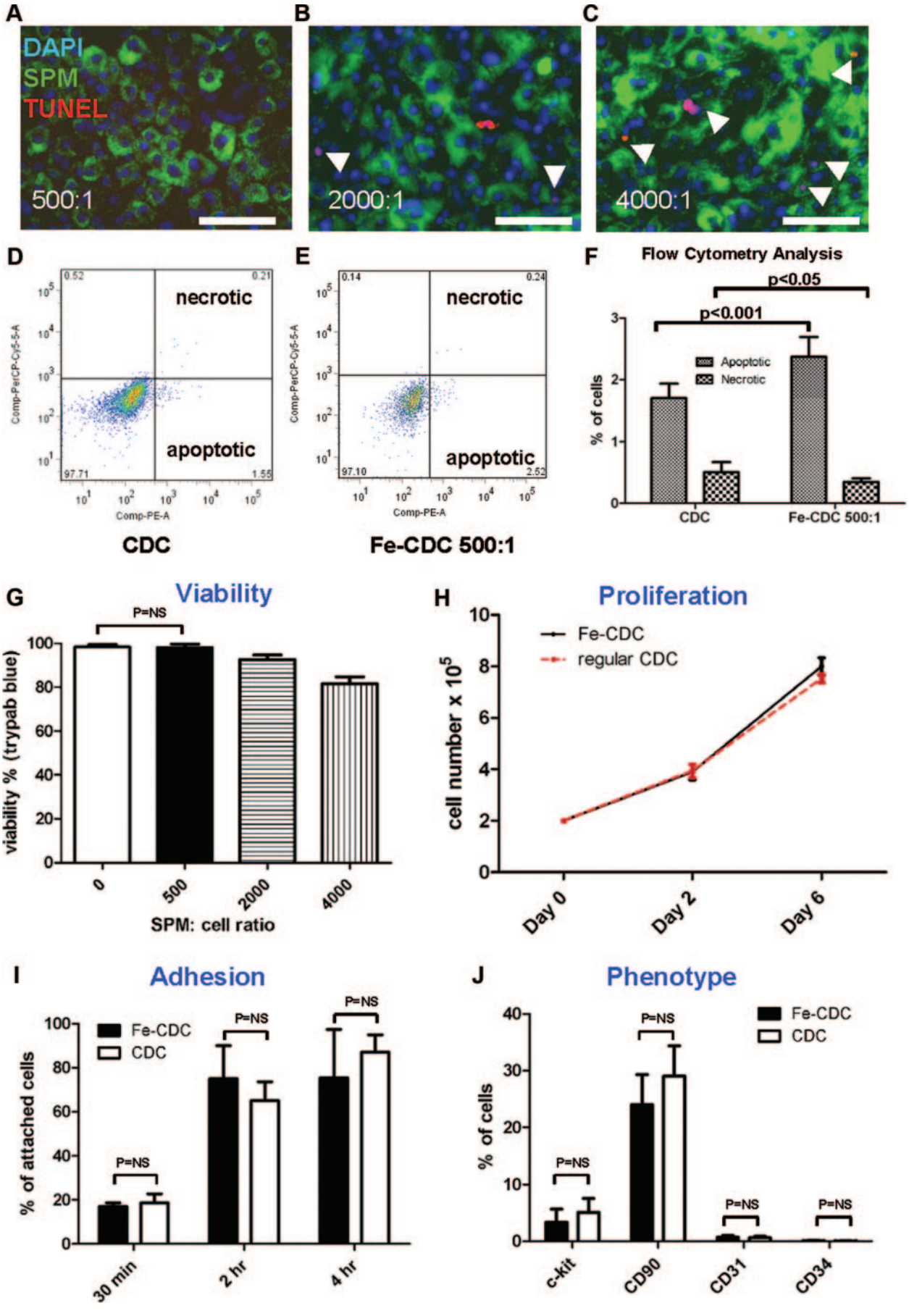

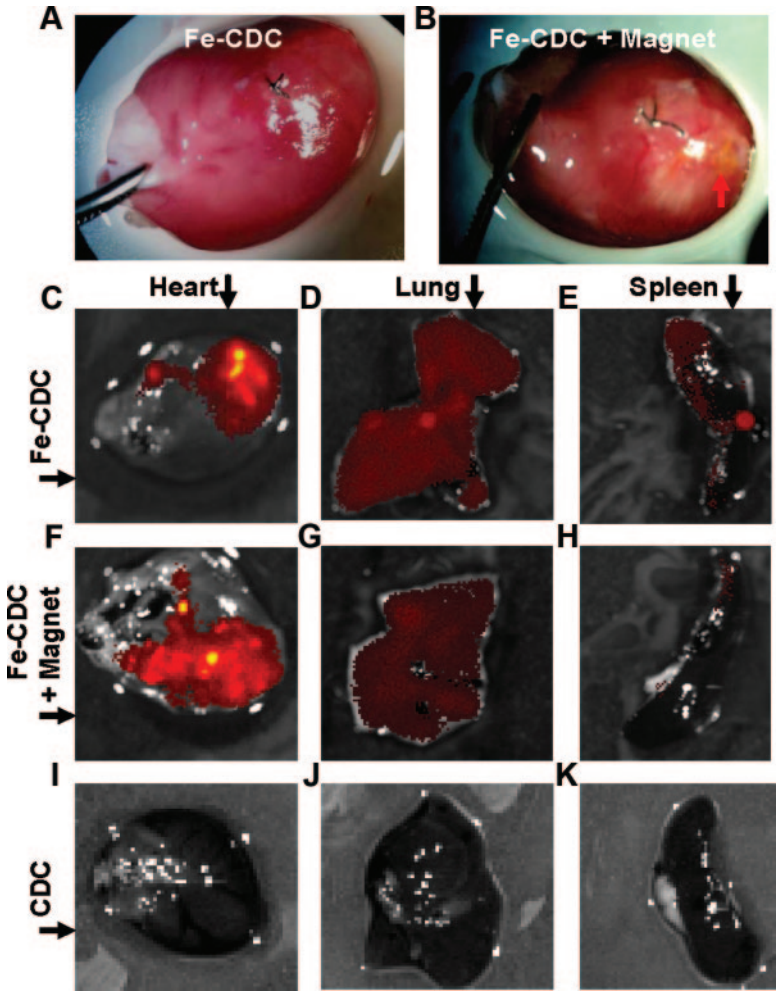

Figure 3. Magnetic targeting increases short-term cell retention in the hearts and reduces off-target migration. A and B, Representative images of hearts from the Fe-CDC and Fe-CDC+magnet group 24 hours after cell injection. Cells are visible as a **yellow-brown area** in the Fe-CDC+magnet group **(B, red arrow)** but not in the Fe-CDC group **(A)**. **C through K,** Representative fluorescence imaging of organs harvested at 24 hours after cell injection. CDCs were labeled with flash-red–conjugated SPMs. Exposure time was set at the same level for each imaging procedure. More fluorescence was detected in a heart from the Fe-CDC+magnet group **(F)** than in the Fe-CDC group **(C)**. Red fluorescence signals were detectable in the lungs and spleens, but less so in the lungs and spleens from the Fe-CDC+magnet group **(G and H)** than in those from the Fe-CDC group **(D and E)**. As a negative control, excised organs from the CDC group (animals were injected with nonlabeled cells) were also imaged; no signals were detected from any such organs **(I through K)**.

(FLI) images revealed more flash-red fluorescence in a heart from the Fe-CDC+magnet group (Figure 3F) than in the Fe-CDC group (Figure 3C). To compare off-target migration, lungs and spleens from the same animals were also harvested and imaged. Not surprisingly, red fluorescence signals were detectable in the lungs, but less so in the lungs from the Fe-CDC+magnet group (Figure 3G) than in those from the Fe-CDC group (Figure 3D). Thus, the magnet retains CDCs in the heart that would otherwise travel elsewhere because of venous dispersion. The fluorescence seen in the Fe-CDC spleen (Figure 3E) may reflect off-target CDCs, or clearance of SPM particles by spleen macrophages. In either case, such fluorescence is markedly reduced in the Fe-CDC+magnet spleen (Figure 3H). As a negative control, excised organs from the CDC group (animals injected with nonlabeled cells) were also imaged. No signals were detectable in any organs (Figure 3I through 3K).

To further assess the numbers of surviving CDCs in the myocardium, quantitative PCR for the male-specific SRY gene was performed. Quantitative PCR results confirmed that magnetic targeting enhanced short-term cell retention in the recipient hearts: the Fe-CDC+magnet group exhibited ≈3-fold greater cell numbers than the Fe-CDC group (Figure 4A). Cell retention was indistinguishable in the Fe-CDC group and the CDC group, confirming the lack of an effect of labeling per se. To examine the effect of magnetic targeting on long-term engraftment, subsets of animals in each group were followed for 3 weeks and then euthanized for quantitative PCR and FLI. Consistent with previous findings,[18,22] PCR results indicated that all 3 groups experienced a huge

Figure 2 (Continued). Effects of SPM labeling on cell death and function. A through C, Microscopy images of TUNEL staining **(red**: apoptotic cells; **green**: SPMs; **blue**: nuclei). CDCs were coincubated with SPMs for 24 hours at varying SPM:cell ratios: 500:1 **(A)**; 2000:1 **(B)**; 4000:1 **(C)**. Apoptotic cells **(red color)** are highlighted with **white arrowheads**. **Bars:** 50 μm. **D and E,** Typical plots of annexin/7-AAD flow cytometry from nonlabeled CDCs **(D)** and SPM-labeled CDCs **(E)**. **F,** Quantification of apoptotic and necrotic cells by flow cytometry (n=9 for CDC; n=8 for Fe-CDC). CDCs were labeled with SPMs for 24 hours and then examined for viability and function. **G,** Viability of SPM-labeled CDCs assessed by trypan blue exclusion. Viability decrease was only observed in the 2000:1 and 4000:1 dosage groups, but not in the 500:1 group. **H,** Proliferation of Fe-CDCs (labeled at 500:1 SPMs) compared with that of control CDCs (n=4). Cell counts at days 0, 2, and 6 were equivalent in the 2 groups. **I,** Adhesion potency of Fe-CDCs (labeled with 500:1 SPMs) compared with that of control CDCs (n=3). Attached cell numbers at 30 minutes, 2 hours, and 4 hours were not statistically different in the 2 groups. **J,** Phenotypic markers c-kit, CD90, CD31, and CD34 from Fe-CDCs (n=8) were compared to those from control CDCs (n=9). No statistical differences were detected for any of those markers.

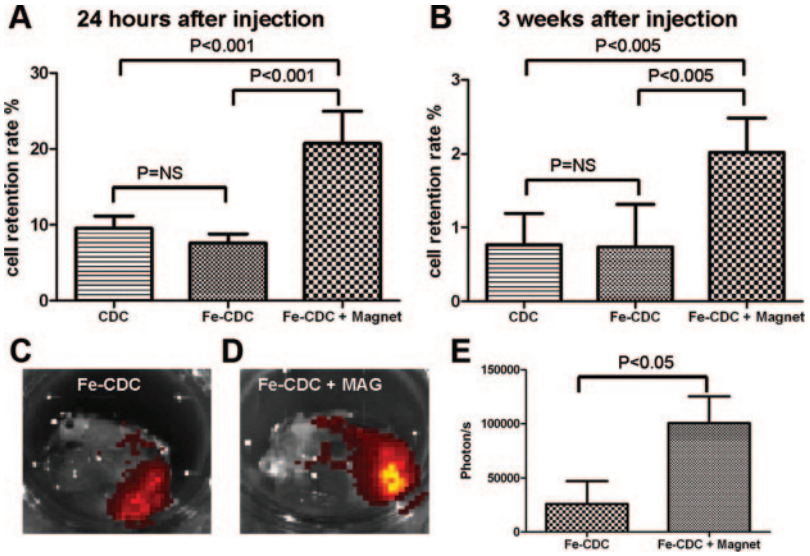

Figure 4. Effects of magnetic targeting on short-term cell retention and long-term cell engraftment. A, Female animals (n=6) were euthanized 24 hours after cell injection. Donor male cells persistent in the female hearts were detected by quantitative PCR for the SRY gene. **B,** Similar PCR experiment performed 3 weeks after injection. **C and D,** CDCs were labeled with flash-red–conjugated SPMs and then injected into animals with **(D)** or without **(C)** magnetic targeting. At 3 weeks after injection, representative hearts from both groups (n=3) were harvested and imaged for detection of flash-red fluorescence. More fluorescence is evident in the Fe-CDC+magnet heart. **E,** Fluorescence intensities (photon/s) from a fixed region of interest (ROI) measured with the Xenogen software.

decrease from the 24-hour time point. However, the Fe-CDC+magnet group still exhibited enhanced cell engraftment relative to the Fe-CDC group (Figure 4B). Again, SPM labeling itself did not affect engraftment, as the Fe-CDC group was comparable to the CDC group. The equivalence of the CDC and Fe-CDC groups at 24 hours (Figure 4A) and 3 weeks (Figure 4B) confirms the idea that SPM labeling does not affect cell proliferation in vivo, assuming the attrition rate of transplanted CDCs is identical in the 2 groups. FLI images showed more flash-red fluorescence in the Fe-CDC+magnet group (Figure 4D) than in the Fe-CDC group (Figure 4C). Fluorescence intensity was ≈4-fold greater in the Fe-CDC+magnet group (Figure 4E). At the 3-week time point, fluorescence intensity will reflect the amount of SPMs in the tissue, but not necessarily the number of engrafted CDCs. By this time, transplanted cells may have died, leaving behind their SPMs in the interstitium or in macrophages; alternatively, exocytosis might allow surviving cells to extrude the particles.[18] Given such considerations, the fact that both PCR and FLI give similar values for "engraftment" is remarkable and quite possibly fortuitous. Nevertheless, it is clear that that magnetic targeting increases both short-term (24 hours) and long-term Fe-CDC engraftment (3 weeks) in the injured myocardium.

Magnetically Targeted Cell Delivery Attenuates Left Ventricular Remodeling and Enhances the Therapeutic Benefit of Cell Transplantation

Morphometric analysis[21] of explanted hearts (n=5 to 6 from each group) at 3 weeks showed severe LV chamber dilatation and infarct wall thinning in PBS-injected hearts (Figure 5A). In contrast, the 3 cell treated groups (Figure 5B through 5D) exhibited attenuated LV remodeling. The protective effect was greatest in the Fe-CDC+magnet group, which had more viable myocardium (Figure 5E) and thicker infarcted walls (Figure 5G), but smaller scars (Figure 5F) and less LV expansion (Figure 5H). The Fe-CDC and CDC groups were indistinguishable in these measures, indicative of a similar treatment effect in those 2 groups.

To investigate whether improved cell retention/engraftment translates to enhanced functional benefit, global LVEF was assessed by echocardiography at baseline (Day 0 after MI and cell injection) and 3 weeks later. LVEF at baseline did not differ between treatment groups, indicating a comparable degree of initial injury (Figure 6A). Over the 3 weeks after infarction, LVEF declined progressively in the control group (PBS-injected animals) (Figure 6A), whereas LVEF improved in all 3 groups receiving CDCs. These results confirm previous data showing that cardiac function can be significantly improved by transplantation of CDCs.[6,17,23,24] Notably, the Fe-CDC+magnet group exhibited better cardiac function compared to either the Fe-CDC group or the CDC group (Figure 6A; $P<0.01$). The LVEFs in the Fe-CDC and CDC groups were indistinguishable, again demonstrating that SPM loading did not undermine the salutary effects of CDCs. To facilitate comparisons among groups, we calculated the treatment effect, ie, the change in LVEF at 3 weeks relative to baseline, in each group (Figure 6B). PBS injection had a negative treatment effect, as the LVEF decreased over time, consistent with previous work.[6,17,23] In contrast, the Fe-CDC+magnet group exhibited a sizable positive treatment effect, greater than that in either the Fe-CDC or CDC groups. The treatment effect in the Fe-CDC group was no different than that in the CDC group. In addition, injection of SPMs alone (no cells) had no beneficial effects (Online Figure IV). To further investigate the relationships between long-term cell retention or myocardial viability on one hand, and cardiac function on the other, 3-week LVEFs were plotted individually against percentages of engraftment (Figure 6C) or viable myocardium in the risk region (Figure 6D) at 3 weeks. Better heart function was clearly associated with higher cell retention rate ($R^2=0.8086$) and increased myocardial viability ($R^2=6282$) by linear regression analysis. These composite functional results indicate that the improved cell retention and engraftment in the Fe-CDC+magnet group indeed translated into superior functional benefit and attenuation of LV remodeling.

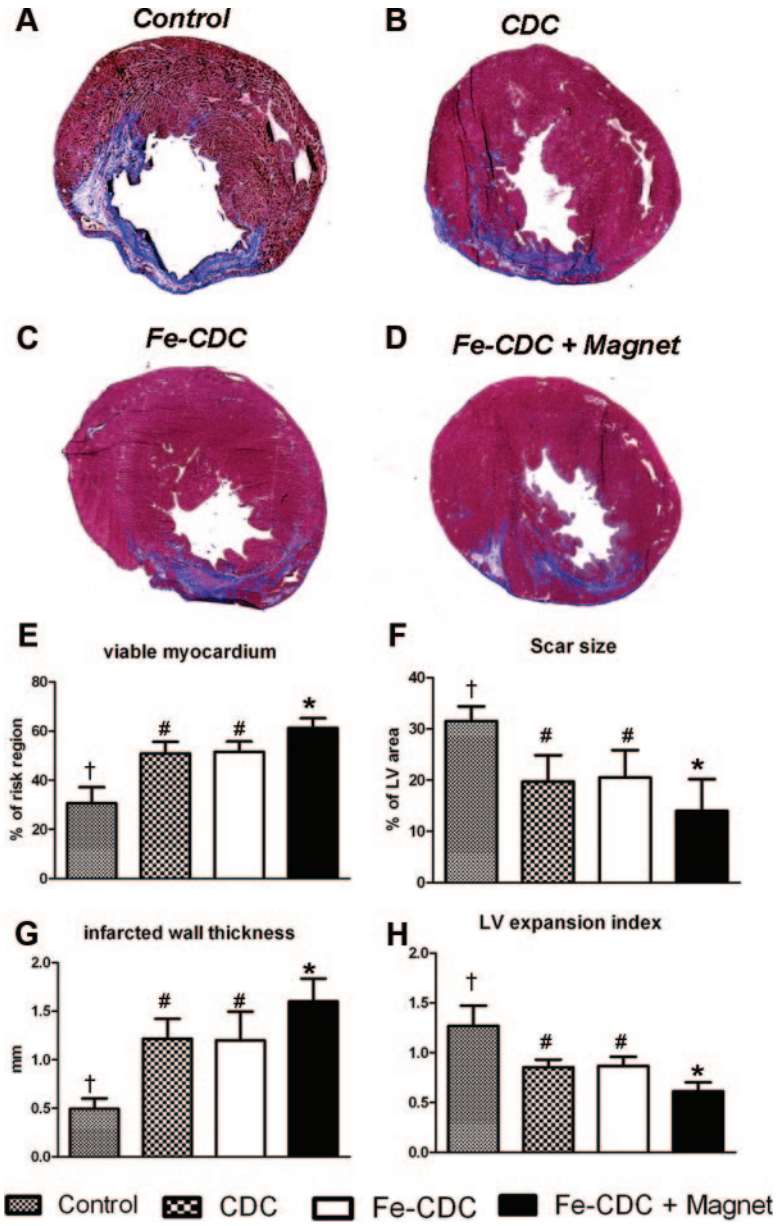

Figure 5. Morphometric heart analysis.
A through D, Representative Masson's trichrome–stained myocardial sections from a subgroup of animals at 3 weeks after treatment (n=6 for Fe-CDC+magnet and Fe-CDC; n=5 for CDC and Control). Scar tissue and viable myocardium are identified in **blue and red color**, respectively.
E through H, Quantitative analysis and LV morphometric parameters (for definition and calculation methods; see the expanded Methods section in the Online Data Supplement). †$P<0.05$ when compared to any other groups; #P=NS; *$P<0.05$ when compared to any other groups.

Magnetic Targeting Enhances Cell Engraftment and Does Not Worsen Inflammation

To further characterize engraftment, hearts from representative animals in each group were harvested 3 weeks after injection and cryo-sectioned for immunohistochemistry. Confocal imaging enabled the detection of transplanted cells (GFP; green); macrophages (CD68; red); and all cell nuclei (DAPI; blue). Figure 7 shows representative confocal images (Fe-CDC+magnet [A]; Fe-CDC [B]; CDC [C]; control [D]). The cell numbers, quantified as positive cells per high-power field (Figure 7E) reveal more GFP-positive cells in the Fe-CDC+magnet group compared to the Fe-CDC or CDC groups. These data agree with the PCR results showing greater long-term cell engraftment with magnetic targeting. Interestingly, GFP-positive multi-cellular clusters were frequently observed in the Fe-CDC+magnet group (Figure 7A). To quantify the effects of magnetic targeting on the spatial distribution of transplanted cells, GFP-positive cells from 50 randomly selected fields (4×10^4 μm^2) were counted and the number of events was plotted against varying cell numbers (Figure 7F). Not surprisingly, most of the fields examined were devoid of transplanted cells in all 3 groups. However, the Fe-CDC+magnet group had more engraftment area (less "empty" area) compared to the Fe-CDC or CDC group ($P<0.05$). The number of fields with 1 to 3 engrafted cells was indistinguishable among all the 3 groups. Interestingly, the Fe-CDC+magnet group had many more fields with 4 to 10 or >10 engrafted cells than the Fe-CDC or CDC group ($P<0.001$). Thus, magnetic targeting increases engraftment in focally condensed patches rather than homogeneously.

One potential concern regarding SPMs and magnetic targeting is the possibility of an inflammatory response, but we found that the tissue density of CD-68$^+$ macrophages was comparable in all 3 groups (Figure 7E). These observations indicate that the presence of SPMs in the host tissue did not cause or worsen inflammation. Notably, at the 3 week time

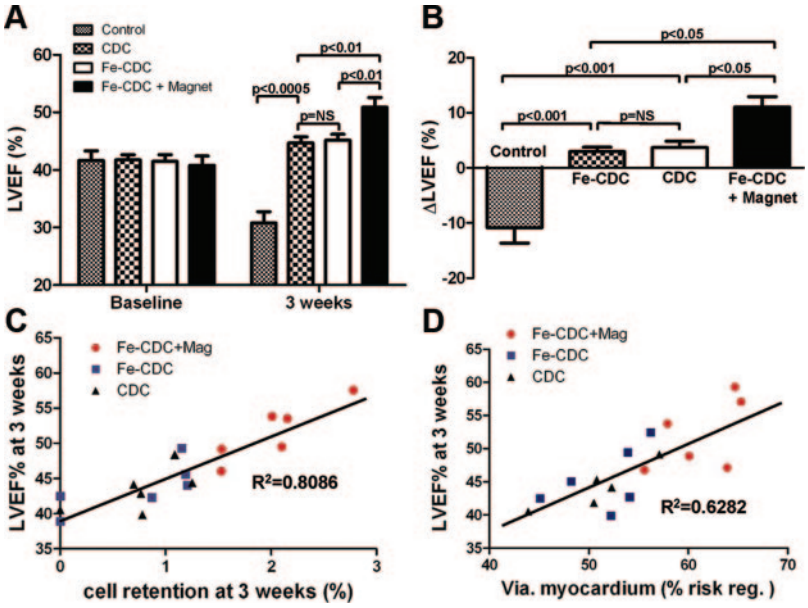

Figure 6. Magnetic targeting enhances functional benefit of CDC transplantation. **A,** LVEF measured by echocardiography at baseline and 3 weeks after cell injection (n=12 for Fe-CDC+magnet and Fe-CDC; n=11 for CDC; n=9 for control). Baseline LVEFs were indistinguishable among the 4 groups. Two-tailed paired Student's *t* test revealed that all 3 cell-treated groups had LVEF improvement, whereas the LVEF from the control group decreased from baseline. The functional improvement was greater in the Fe-CDC+magnet group than in the others. **B,** Changes of LVEF from baseline in each group. Values are expressed as means±SEM. **C and D,** Three-week LVEFs were plotted against 3-week cell retention rates and viable myocardium in the risk region, from each animal in each group for which both sets of data were available. Linear regression was performed.

point the majority of GFP-positive cells are SPM-negative; only ≈10% of transplanted cells still contained SPMs. A shift of SPMs from the transplanted CDCs to resident macrophages was clearly evident when sections were compared at 24 hours versus 3 weeks (Online Figure V). These observations are consistent with the concept that Fe-CDCs expel SPMs via exocytosis in vivo, as occurs with other iron-labeled stem cells,[25–27] followed by endocytosis by macrophages and eventual incorporation into body's iron stores.[28]

We have found that CDCs improve cardiac function both by direct regeneration and by indirect mechanisms.[24] To assess whether transplanted Fe-CDCs differentiate, we stained for cardiac (α-sarcomeric actin) and endothelial (von Willebrand factor) markers. GFP^+/α-sarcomeric actin $(SA)^+$ cells were consistently detected (Figure 8A), indicating the ability of transplanted cells to differentiate into cardiomyocytes. The Fe-CDC+magnet group had more $GFP^+/\alpha\text{-}SA^+$ and $GFP^-/\alpha\text{-}SA^+$ cells than the CDC or Fe-CDC group (Figure 8B and 8C). The increase in $GFP^+/\alpha\text{-}SA^+$ cells attests to the creation of new myocardium by direct differentiation, whereas the increase in $GFP^-/\alpha\text{-}SA^+$ cells likely reflects indirect mechanisms (recruitment of endogenous regeneration and/or tissue preservation).[21,24,29] To further dissect the mechanism of benefit of magnetic targeting, we quantified the magnet-related increment in various cell populations: recipient-derived myocytes, mature donor-derived myocytes, and immature donor-derived myocytes (Figure 8D). Binucleation was used to distinguish between mature and immature myocytes[30]; such myocytes were distinctly longer than mononucleated myocytes, with a typical length: width ratio >3:1. Direct regeneration ($GFP^+/\alpha\text{-}SA^+$ cells) contributed 17.7% of the total benefit; of that percentage, an absolute 7.3% was comprised of mature donor-derived myocytes. In relative terms, 41.2% of the total donor-derived myocytes were binucleated. The quantitative data also suggest that SPM labeling has minimal impact on in vivo cardiac differentiation, as the CDC and Fe-CDC groups had similar densities of $GFP^+/\alpha\text{-}SA^+$ cells (Figure 8B). In addition, remnant SPMs in the cytoplasm did not prevent Fe-CDCs from differentiating into a cardiomyocyte phenotype, as SPM/GFP/α-SA triple positive cells were detected (Online Figure VI; highlighted with white solid arrowheads). Endothelial differentiation was also confirmed by the presence of GFP^+/von Willebrand factor–positive cells (Online Figure VII).

Discussion

One of the main hurdles for cellular cardiomyoplasty is the low, variable retention of transplanted cells.[6,7,31] Many injected cells are lost because of the combination of tissue blood flow (washing out cells) and cardiac contraction (squeezing out cells).[6] Here, we have demonstrated that brief (10 minutes) magnetic attraction successfully attenuates cell loss during injection. Notably, this transient magnetic targeting seemed to have a "butterfly effect" on subsequent cell therapy outcomes: both functional benefit (Figure 6) and long-term cell engraftment (Figure 7) were enhanced. We rationalize these findings as follows (see Figure 8E for a schematic): magnetic targeting improved short-term cell retention (Figure 4A), which boosted long-term engraftment (Figures 4B and 7A). The enhanced engraftment translated into greater therapeutic benefit (Figure 6) by both indirect (paracrine) and direct regeneration mechanisms, with the former as the dominant factor (Figure 8D). We also found that some of the CDCs surviving at 3 weeks appear in multi-cellular clusters (Figure 7A and 7F) in the Fe-CDC+magnet group, which we speculate may reflect a condensation effect of magnetic targeting. Three-dimensional multicellular clusters are generally more resistant to hostile environments, such as the infarcted myocardium, providing mechanical and paracrine support to transplanted neighbors.[32,33]

This is the first study to report magnetically targeted cell therapy for enhanced myocardial regeneration. Previous investigations of magnetically targeted cell delivery for cardiovascular applications are limited to endothelial-related cell

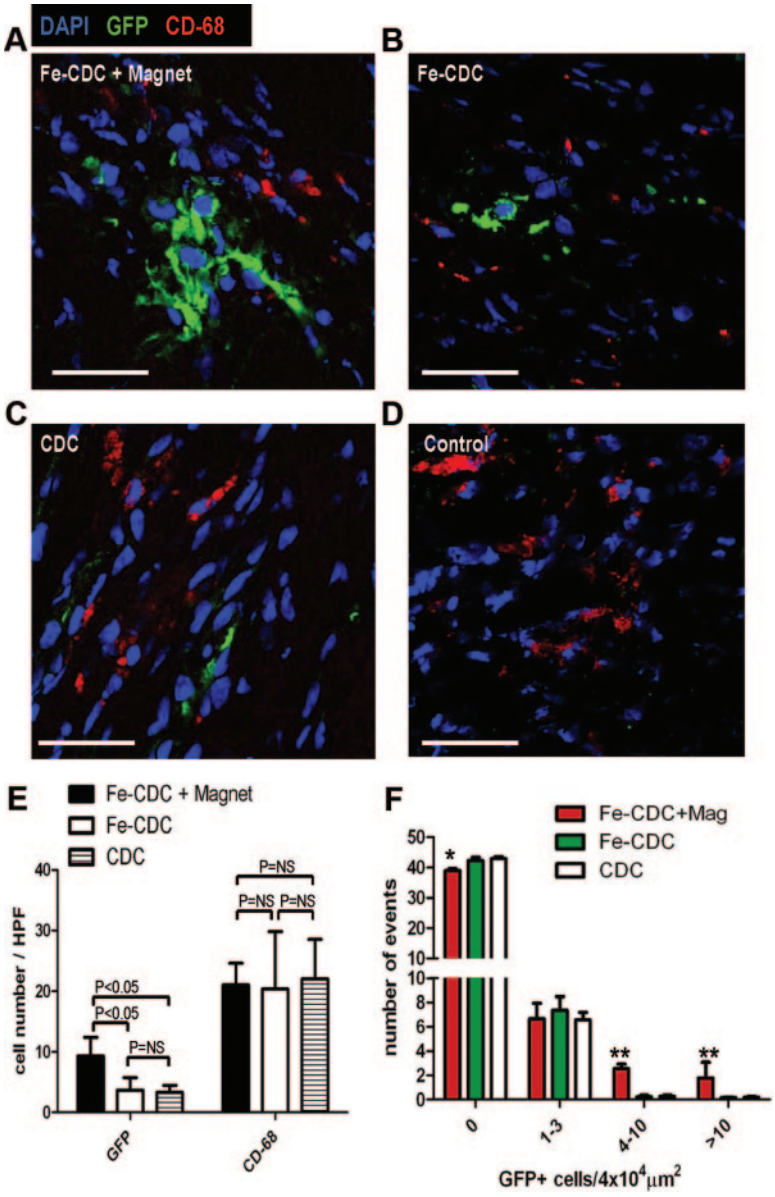

Figure 7. Histological analysis of cell engraftment and inflammatory response. At 3 weeks after cell transplantation, hearts from representative animals (n=5 to 6) in each group were harvested and frozen-sectioned for histological analysis. Sections from different depths of the heart were stained for CD-68 (macrophages) and counter-stained with DAPI. Confocal imaging was performed for simultaneous detection of transplanted cells (GFP; **green**) and macrophages (CD-68; **red**): Fe-CDC+magnet **(A)**; Fe-CDC **(B)**; CDC **(C)**; control **(D)**. **Bars:** 100 μm. **E,** GFP-positive cell and macrophage numbers from 6 randomly selected high-power fields (3 from infarct area and 3 from periinfarct area) on each section were quantified. **F,** GFP-positive cells in 50 randomly selected fields ($4\times10^4\mu m^2$) were counted. The number of events was plotted against varying GFP-positive cell numbers. $^{**}P<0.01$, $^{*}P<0.05$ when compared to the CDC or Fe-CDC group.

therapies such as stent endothelialization or vascular repair.[9–14] In those cases, rheological forces in large-bore vessels are the major obstacle for magnetic targeting to counter. In a myocardial infarction model, venous efflux is potentiated by the squeezing effect of cardiac contraction. We showed that magnetic targeting can offset the forces driving injected cells out of the myocardium, thereby improving cell engraftment. In addition, previous studies limited their investigation to comparisons of acute cell targeting or retention, without examining possible functional benefits of magnetic targeting. We found that higher cell retention indeed translates into higher engraftment and greater functional improvement downstream. Indeed, the quantitative relationship between engraftment and LV function is striking (Figure 6C), validating the strategy of boosting cell retention as a means to enhance functional benefit.

The SPMs used in the present studies represent a class of superparamagnetic iron oxides (SPIOs). Food and Drug Administration–approved SPIOs are nontoxic and biocompatible and have been used as MRI contrast agents in human subjects.[28,34] Consistent with the literature,[9,10] our in vitro toxicity data confirmed that micron-size SPIOs had a good safety profile, as they did not significantly alter cell viability, proliferation, adhesion, apoptosis, or antigenic phenotype (Figure 2). Also, SPM labeling did not undermine Fe-CDC proliferation (Figure 4A and 4B) or the potential for cardiac and endothelial differentiation (Online Figures VI and VII) in vivo. These findings are consistent with previous characterization of SPIOs in embryonic stem cells.[35] Magnetic targeting did not increase macrophage infiltration (Figure 7E), consistent with previous work.[36,37] The potential for chemical toxicity of parenteral iron has also been well documented.[38] Iron from injected SPMs will eventually be incorporated into the body's own iron stores. The total amount of iron oxide for diagnostic imaging (40 to 200 mg of Fe) is small compared to the total human iron stores (≈3500 mg). The amount needed

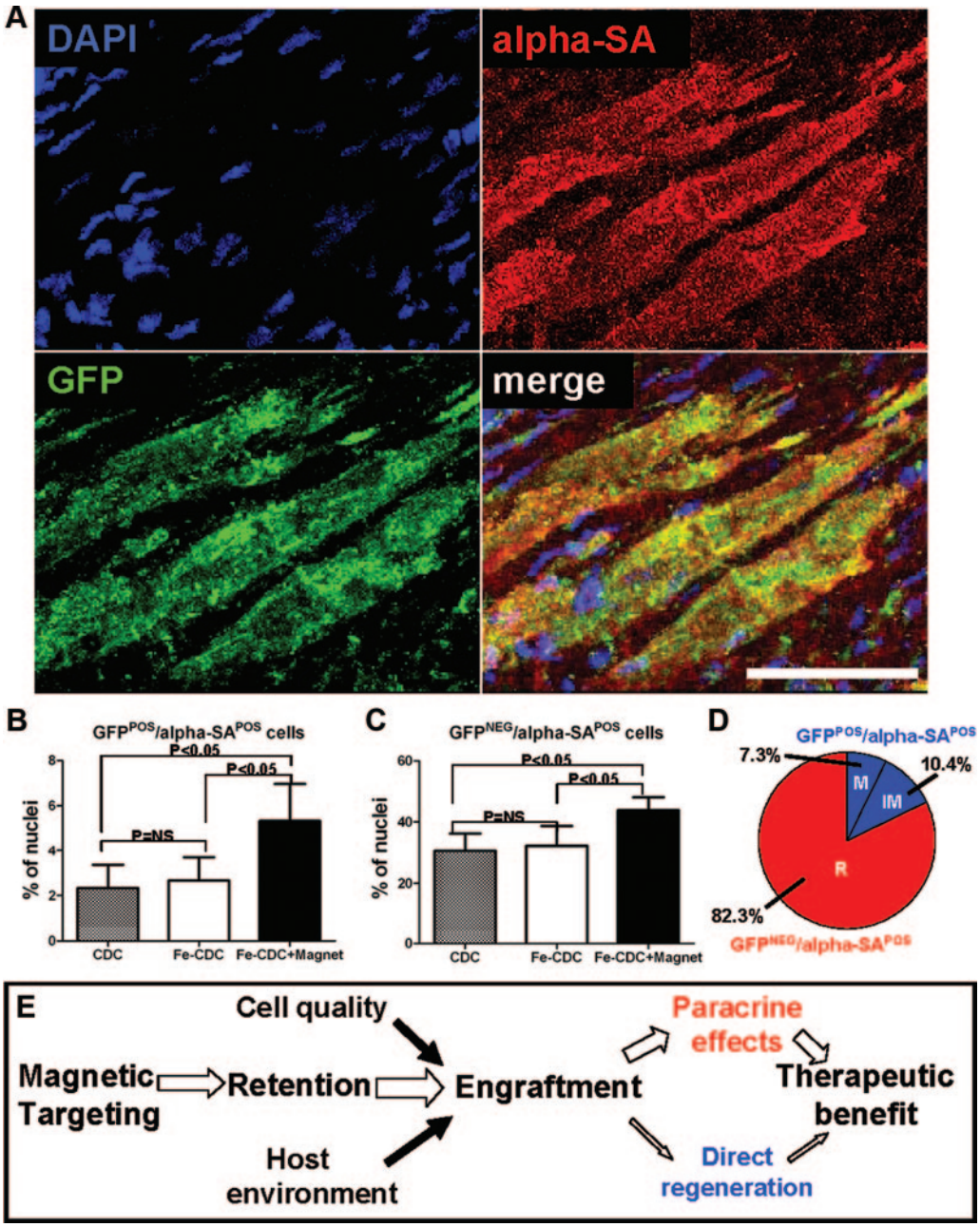

Figure 8. Cardiac differentiation of transplanted CDCs. A, Representative confocal micrographs from a heart in the Fe-CDC+magnet group showing cells expressing GFP **(green)** and α-SA **(red)**. The colocalization of GFP with α-SA indicates that transplanted CDCs participated in regeneration of myocardium, differentiating into a cardiomyocyte phenotype. **B and C,** Quantification of the density of $GFP^+/\alpha\text{-}SA^+$ and $GFP^-/\alpha\text{-}SA^+$ cells in the regions where GFP cells engrafted. **D,** Percentage distribution of recipient and donor myocytes (both mature and immature) in the increment from the Fe-CDC group to the Fe-CDC+magnet group is quantified. M indicates mature donor-derived cardiomyocytes; IM, immature donor-derived cardiomyocytes; R, recipient-derived cardiomyocytes. **E,** Potential mechanism of magnetic targeting–enhanced cell therapy. **Bar:** 50 μm.

for magnetically targeted cell therapy will likely be even smaller. For instance, in the ongoing phase I clinical trial CADUCEUS (see www.clinicaltrials.org), we give a maximum of 25 million CDCs to each study subject. Based on the fact that every SPM particle contains 0.5 pg of iron oxides and a 500:1 SPM to cell ratio is used, only 5 mg of Fe would be administered to each patient treated with such a protocol.

We used direct myocardial injection in this study because it is a well-characterized cell delivery method in small animal models. However, less-invasive routes such as intravenous or intracoronary delivery also stand to benefit from magnetic targeting. Such routes of delivery yield even lower cell retention rates than direct myocardial injection.[39,40] In pondering the translation of our results to a clinical setting, we envision noninvasive exposure to magnetic fields near the heart while cell delivery is performed. The external magnetic field may be generated as simply as by applying a fixed magnet to the patient's chest, although machines that focus and potentially shape the magnetic field may enable more refinement, extending to specific regions within the body (eg,

the posterior wall of the heart).[41] Electromagnetic catheters represent another potential means of focused field generation within defined regions of the body.

We conclude that magnetic targeting enhances cell retention, engraftment and functional benefit in a rat myocardial infarction model. Although it describes a new and promising method, the present study has a number of limitations: we have used only a proof-of-concept small animal model; further optimization is needed to find the best magnetic strength and duration for effective targeting; and large-animal data are necessary to advance the process of translation. In addition, rather than optimizing basal cell dosage, we chose a number consistent with various prior studies[6,21,42] that had shown functional benefit in small animals. We recognize that the dosages used here may not be readily scalable to the clinical setting. Further dosage optimization would be valuable, both in small- and large-animal models, to inform future clinical studies.

Acknowledgments

We thank Christy Houde, Supurna Chowdhury, and Giselle Galang for technical assistance. We also thank Drs John Terrovitis and Rachel Smith for helpful discussions.

Sources of Funding

This work was supported by NIH grant R01 HL083109.

Disclosures

E.M. is a founder and equity holder in Capricor Inc. Capricor provided no funding for the present study. The remaining authors report no conflicts.

References

1. Wollert KC, Drexler H. Clinical applications of stem cells for the heart. *Circ Res*. 2005;96:151–163.
2. Fukushima S, Varela-Carver A, Coppen SR, Yamahara K, Felkin LE, Lee J, Barton PJR, Terracciano CMN, Yacoub MH, Suzuki K. Direct intramyocardial but not intracoronary injection of bone marrow cells induces ventricular arrhythmias in a rat chronic ischemic heart failure model. *Circulation*. 2007;115:2254–2261.
3. Robey TE, Saiget MK, Reinecke H, Murry CE. Systems approaches to preventing transplanted cell death in cardiac repair. *J Mol Cell Cardiol*. 2008;45:567–581.
4. Ye L, Haider HK, Guo C, Sim EKW. Cell-based VEGF delivery prevents donor cell apoptosis after transplantation. *Ann Thorac Surg*. 2007;83:1233–1234.
5. Zhang M, Methot D, Poppa V, Fujio Y, Walsh K, Murry CE. Cardiomyocyte grafting for cardiac repair: graft cell death and anti-death strategies. *J Mol Cell Cardiol*. 2001;33:907–921.
6. Terrovitis J, Bonios M, Fox J, Engles JM, Yu J, Leppo MK, Pomper MG, Wahl RL, Seidel J, Tsui BM, Bengel FM, Abraham R, Marban E. Noninvasive quantification and optimization of acute cell retention by in vivo positron emission tomography after intramyocardial cardiac-derived stem cell delivery. *J Am Coll Cardiol*. 2009;54:1619–1626.
7. Teng CJ, Luo J, Chiu RCJ, Shum-Tim D. Massive mechanical loss of microspheres with direct intramyocardial injection in the beating heart: implications for cellular cardiomyoplasty. *J Thorac Cardiovasc Surg*. 2006;132:628–632.
8. Polyak B, Friedman G. Magnetic targeting for site-specific drug delivery: applications and clinical potential. *Expert Opin Drug Deliv*. 2009;6:53–70.
9. Pislaru SV, Harbuzariu A, Agarwal G, Witt Aas Cvt Latg T, Gulati R, Sandhu NP, Mueske Aa C, Kalra M, Simari RD, Sandhu GS Magnetic forces enable rapid endothelialization of synthetic vascular grafts. *Circulation.* 2006;114:I-314–318.
10. Pislaru SV, Harbuzariu A, Gulati R, Witt T, Sandhu NP, Simari RD, Sandhu GS. Magnetically targeted endothelial cell localization in stented vessels. *J Am Coll Cardiol*. 2006;48:1839–1845.
11. Polyak B, Fishbein I, Chorny M, Alferiev I, Williams D, Yellen B, Friedman G, Levy RJ. High field gradient targeting of magnetic nanoparticle-loaded endothelial cells to the surfaces of steel stents. *Proc Natl Acad Sci U S A*. 2008;105:698–703.
12. Singh JP. Enabling technologies for homing and engraftment of cells for therapeutic applications. *JACC Cardiovasc Interv*. 2009;2:803–804.
13. Kyrtatos PG, Lehtolainen P, Junemann-Ramirez M, Garcia-Prieto A, Price AN, Martin JF, Gadian DG, Pankhurst QA, Lythgoe MF. Magnetic tagging increases delivery of circulating progenitors in vascular injury. *JACC Cardiovasc Interv*. 2009;2:794–802.
14. Consigny P, Silverberg D, Vitali N. Use of endothelial cells containing superparamagnetic microspheres to improve endothelial cell delivery to arterial surfaces after angioplasty. *J Vasc Interv Radiol*. 1999;10:155–163.
15. Davis DR, Zhang Y, Smith RR, Cheng K, Terrovitis J, Malliaras K, Li T-S, White A, Makkar R, Marban E. Validation of the cardiosphere method to culture cardiac progenitor cells from myocardial tissue. *PLoS ONE*. 2009;4:e7195.
16. Messina E, De Angelis L, Frati G, Morrone S, Chimenti S, Fiordaliso F, Salio M, Battaglia M, Latronico MVG, Coletta M, Vivarelli E, Frati L, Cossu G, Giacomello A. Isolation and expansion of adult cardiac stem cells from human and murine heart. *Circ Res*. 2004;95:911–921.
17. Smith RR, Barile L, Cho HC, Leppo MK, Hare JM, Messina E, Giacomello A, Abraham MR, Marban E. Regenerative potential of cardiosphere-derived cells expanded from percutaneous endomyocardial biopsy specimens. *Circulation*. 2007;115:896–908.
18. Terrovitis J, Stuber M, Youssef A, Preece S, Leppo M, Kizana E, Schar M, Gerstenblith G, Weiss RG, Marban E, Abraham MR. Magnetic resonance imaging overestimates ferumoxide-labeled stem cell survival after transplantation in the heart. *Circulation*. 2008;117:1619–1626.
19. Kanoh M, Takemura G, Misao J, Hayakawa Y, Aoyama T, Nishigaki K, Noda T, Fujiwara T, Fukuda K, Minatoguchi S, Fujiwara H. Significance of myocytes with positive DNA in situ nick end-labeling (TUNEL) in hearts with dilated cardiomyopathy: not apoptosis but DNA repair. *Circulation*. 1999;99:2757–2764.
20. Cheng Z, Levi J, Xiong Z, Gheysens O, Keren S, Chen X, Gambhir SS. Near-infrared fluorescent deoxyglucose analogue for tumor optical imaging in cell culture and living mice. *Bioconjug Chem*. 2006;17:662–669.
21. Tang X-L, Rokosh G, Sanganalmath SK, Yuan F, Sato H, Mu J, Dai S, Li C, Chen N, Peng Y, Dawn B, Hunt G, Leri A, Kajstura J, Tiwari S, Shirk G, Anversa P, Bolli R. Intracoronary administration of cardiac progenitor cells alleviates left ventricular dysfunction in rats with a 30-day-old infarction. *Circulation*. 2010;121:293–305.
22. Li Z, Lee A, Huang M, Chun H, Chung J, Chu P, Hoyt G, Yang P, Rosenberg J, Robbins RC, Wu JC. Imaging survival and function of transplanted cardiac resident stem cells. *J Am Coll Cardiol*. 2009;53:1229–1240.
23. Johnston PV, Sasano T, Mills K, Evers R, Lee S-T, Smith RR, Lardo AC, Lai S, Steenbergen C, Gerstenblith G, Lange R, Marban E. Engraftment, differentiation, and functional benefits of autologous cardiosphere-derived cells in porcine ischemic cardiomyopathy. *Circulation*. 2009;120:1075–1083.
24. Chimenti I, Smith RR, Li T-S, Gerstenblith G, Messina E, Giacomello A, Marban E. Relative roles of direct regeneration versus paracrine effects of human cardiosphere-derived cells transplanted into infarcted mice. *Circ Res.* 2010;106:971–980.
25. Arbab AS, Jordan EK, Wilson LB, Yocum GT, Lewis BK, Frank JA. In vivo trafficking and targeted delivery of magnetically labeled stem cells. *Hum Gene Ther*. 2004;15:351–360.
26. Arbab AS, Bashaw LA, Miller BR, Jordan EK, Lewis BK, Kalish H, Frank JA. Characterization of biophysical and metabolic properties of cells labeled with superparamagnetic iron oxide nanoparticles and transfection agent for cellular MR imaging. *Radiology*. 2003;229:838–846.
27. Wang YXJ, Wang HH, Au DWT, Zou BS, Teng LS. Pitfalls in employing superparamagnetic iron oxide particles for stem cell labelling and in vivo MRI tracking. *Br J Radiol.* 2008;81:987-a-988.
28. Thorek D, Chen A, Czupryna J, Tsourkas A. Superparamagnetic iron oxide nanoparticle probes for molecular imaging. *Ann Biomed Eng*. 2006;34:23–38.
29. Gnecchi M, Zhang Z, Ni A, Dzau VJ. Paracrine mechanisms in adult stem cell signaling and therapy. *Circ Res*. 2008;103:1204–1219.
30. Chen X, Wilson RM, Kubo H, Berretta RM, Harris DM, Zhang X, Jaleel N, MacDonnell SM, Bearzi C, Tillmanns J, Trofimova I, Hosoda T, Mosna F, Cribbs L, Leri A, Kajstura J, Anversa P, Houser SR. Adolescent

feline heart contains a population of small, proliferative ventricular myocytes with immature physiological properties. *Circ Res*. 2007;100:536–544.
31. Al Kindi A, Ge Y, Shum-Tim D, Chiu RC. Cellular cardiomyoplasty: routes of cell delivery and retention. *Front Biosci*. 2008;13:2421–2434.
32. Ruei-Zhen Lin H-YC. Recent advances in three-dimensional multicellular spheroid culture for biomedical research. *Biotechnol J*. 2008;3:1172–1184.
33. Chung-Chi W, Chun-Hung C, Shiaw-Min H, Wei-Wen L, Chih-Hao H, Wen-Yu L, Yen C, Hsing-Wen S. Spherically symmetric mesenchymal stromal cell bodies inherent with endogenous extracellular matrices for cellular cardiomyoplasty. *Stem Cells*. 2009;27:724–732.
34. Corot C, Robert P, Idée J-M, Port M. Recent advances in iron oxide nanocrystal technology for medical imaging. *Adv Drug Deliv Rev*. 2006;58:1471–1504.
35. Au K-W, Liao S-Y, Lee Y-K, Lai W-H, Ng K-M, Chan Y-C, Yip M-C, Ho C-Y, Wu EX, Li RA, Siu C-W, Tse H-F. Effects of iron oxide nanoparticles on cardiac differentiation of embryonic stem cells. *Biochem Biophys Res Commun.* 2009;379:898–903.
36. Bourrinet PP, Bengele HHP, Bonnemain BP, Dencausse AP, Idee J-MP, Jacobs PMBSP, Lewis JMP. Preclinical safety and pharmacokinetic profile of ferumoxtran-10, an ultrasmall superparamagnetic iron oxide magnetic resonance contrast agent. *Invest Radiol*. 2006;41:313–324.
37. Raynal IP, Prigent PP, Peyramaure SBS, Najid AP, Rebuzzi CMS, Corot CP. Macrophage endocytosis of superparamagnetic iron oxide nanoparticles: mechanisms and comparison of ferumoxides and ferumoxtran-10. *Invest Radiol*. 2004;39:56–63.
38. Bonnemain B. Superparamagnetic agents in magnetic resonance imaging: physicochemical characteristics and clinical applications. A review. *J Drug Target*. 1998;6:167–174.
39. Freyman T, Polin G, Osman H, Crary J, Lu M, Cheng L, Palasis M, Wilensky RL. A quantitative, randomized study evaluating three methods of mesenchymal stem cell delivery following myocardial infarction. *Eur Heart J.* 2006;27:1114–1122.
40. Hou D, Youssef EA, Brinton TJ, Zhang P, Rogers P, Price ET, Yeung AC, Johnstone BH, Yock PG, March KL. Radiolabeled cell distribution after intramyocardial, intracoronary, and interstitial retrograde coronary venous delivery: implications for current clinical trials. *Circulation.* 2005;112(9 Suppl):I-150–I-156.
41. Ernst S, Ouyang F, Linder C, Hertting K, Stahl F, Chun J, Hachiya H, Bansch D, Antz M, Kuck K-H. Initial experience with remote catheter ablation using a novel magnetic navigation system: magnetic remote catheter ablation. *Circulation.* 2004;109:1472–1475.
42. Haider HK, Jiang S, Idris NM, Ashraf M. IGF-1-overexpressing mesenchymal stem cells accelerate bone marrow stem cell mobilization via paracrine activation of SDF-1{alpha}/CXCR4 signaling to promote myocardial repair. *Circ Res*. 2008;103:1300–1308.

Novelty and Significance

What Is Known?

- When cells are injected into the heart, the retention of injected cells in the tissue is low, potentially restricting the therapeutic benefit of cardiomyoplasty.
- Cardiosphere-derived cells (CDCs) improve cardiac function in the injured heart and exhibit multilineage potential.
- Although CDCs can engraft and differentiate into cardiomyocytes and vascular cells in the injured heart, most of their therapeutic benefit is attributable to indirect ("paracrine") mechanisms rather than to direct regeneration.

What New Information Does This Article Contribute?

- Loading cardiosphere-derived cells with iron oxide particles renders them susceptible to magnetic attraction but does not interfere with their viability or function.
- Brief external magnetic field application as an adjunct to magnetized CDC injection ("magnetic targeting") triples short-term retention as well as long-term engraftment.
- Adverse remodeling of the heart is attenuated, viability is enhanced, and ventricular function is greater with magnetic targeting.
- Greater cell retention leads to superior benefits via scaling of previously described mechanisms (paracrine effects plus a minor contribution of direct regeneration).

The success of stem cell therapies for heart disease is limited by low transplanted cell retention in the tissue, due at least in part to washout via coronary veins. We sought to counter the efflux of transplanted cells by rendering them magnetically responsive and imposing an external magnetic field on the heart during and immediately after injection. CDCs were labeled with superparamagnetic microspheres, a process which did not undermine cell viability or function. Labeled rat CDCs were injected into the peri-infarct region in rats undergoing acute myocardial infarction. When a magnet was superimposed on the surgical field to achieve magnetic targeting, cells were visibly attracted toward the magnet and accumulated around the ischemic zone. In contrast, the majority of nontargeted cells washed out immediately after injection. More transplanted cells were retained in the heart, and fewer migrated into other organs, with magnetic targeting; adverse ventricular remodeling was attenuated, and functional improvement was superior. This simple, novel method to improve injected cell retention is readily generalizable and offers the potential for rapid translation to clinical applications.

Supplemental Materials

Detailed Methods

Rat CDC culture

Rat hearts were excised and biopsies of the left ventricle were cut into 1 to 3 mm^3 pieces with a sterile scalpel. The minced tissues were digested with 0.25% trypsin (Invitrogen, Carlsbad, CA, USA) for 5-10 min and then cultured on fibronectin-coated tissue culture dishes using media consisting of Iscove's Modified Dulbecco's Medium (IMDM, Invitrogen) supplemented with 20% fetal bovine serum (FBS), 100 U/mL penicillin G, 100 µg/mL streptomycin, and 0.1 mmol/L 2-mercaptoethanol. This media was referred to as cardiosphere media (CEM). After 10-20 days, a layer of fibroblast-like adherent cells and a smaller number of phase-bright cells migrated from the tissue explants. The cells were washed with PBS and detached with TrypLE^{TM} Select (Invitrogen) at room temperature. The harvested cells were then seeded into poly-D-lysine coated 6-well plates ($1x10^5$ cells/well), in CEM containing 10% FBS. Under this suspension culture condition, the cells self-aggregate into cardiospheres in 3-10 days. These cardiospheres were harvested, seeded in fibronectin-coated tissue culture flasks for expansion as monolayers in CEM containing 20% FBS. These cells express several stem cell markers and are referred to as cardiosphere-derived cells or CDCs.

SPM labelling and *in vitro* toxicity experiment

After 2 passages, rat CDCs were labelled with Dragon-green fluorescence-conjugated SPM particles by co-incubation of the cells with SPMs for 24 hr. For assessment of cell proliferation, 200,000 SPM-labelled and non-labelled cells were seeded into T25 tissue culture flasks. After 2 and 6 days of culture, cells were harvested from the flasks and

viable cells were manually counted by Trypan Blue exclusion to determine the proliferative activity of CDCs. For assessment of cell adhesion activity, both SPM-labelled and control cells were seeded at the same initial density onto fibronectin-coated dishes. At 30 min, 2 hours and 4 hours after cell seeding, the media was removed and the flask washed by PBS 3 times to remove floating cells. Attached cells were then harvested, counted and quantified as a percentage of the initial seeding number. Cell apoptosis and necrosis were assessed by TUNEL staining (In Situ Cell Death Detection Kit, TMR red, Roche, Germany). Reactive oxygen species (ROS) fluorescence was detected by confocal imaging using the Image-iT™ LIVE Green Reactive Oxygen Species Detection Kit (Invitrogen). Quantitative ROS measurement was performed by staining cells with 6-carboxy-2',7'-dichlorodihydrofluorescein diacetate di(acetoxymethyl ester) (Invitrogen) and then measuring fluorescence intensity with a SpectraMax M5 plate reader (Molecular Devices, Sunnyvale, CA). Plain CDCs and H_2O_2-treated CDCs were included as negative and positive controls, respectively.

Flow cytometry

Flow cytometry experiments were performed using a LSRII equipment (BD Biosciences, San Jose, CA). Monoclonal antibodies were conjugated with fluorophores using commercially available kits (Molecular Probes, Eugene, OR). Flow cytometry analysis of cell apoptosis/necrosis was performed with the Annexin V-PE Apoptosis Detection Kit I (BD Pharmingen 559763). For phenotypic characterization, the following monoclonal antibodies and conjugated fluorochromes were used with corresponding isotype controls: CD31 (BD Pharmingen 555445), CD34 (Chemicon CBL555F); CD90-FITC (Dianova

DIA120); c-Kit (BD Pharmingen 550412). Fluorescent compensation was included using single-labeled controls. The percentage of positive cells was defined as the percent of the population falling above the 99th percentile of an isotype control cell population. Data analysis was performed using flow cytometry software (Flow-Jo 7.2.2 Treestar Inc., Ashland, OR).

Animal model

Animal care was in accordance to Institutional Animal Care and Use Committee guidelines. Female WKY rats (Charles River Laboratories, Wilmington, MA) (n=88 total) underwent left thoracotomy in the 4th intercostal space under general anesthesia. The heart was exposed and myocardial infarction was produced by permanent ligation of the left anterior descending coronary artery, using a 9-0 silk suture, immediately before cell injection. CDCs (total of 1 million; SPM-labeled or non-labeled; suspended in 100 µl of PBS) were injected directly into the myocardium, at 4 sites into the border zone of infarction (i.e., 250,000 cells in 25 µl PBS per site), using a 29G needle. For magnetic targeting, a 1.3 Tesla circular NdFeB magnet (Edmund Scientifics, Tonawanda, NY) was placed above the heart on the retractor (Online Movie II) during and 10 min after the cell injection. The chest was closed and animal was allowed to recover after all procedures.

Fluorescence imaging

Representative animals from each cell-injected group were euthanized at 24 hours and 3 weeks after cell injection for fluorescence imaging purposes. The heart, lung and spleen were harvested. Organs were placed in an IVIS 200 imaging system (previously

Xenogen Corporation; now Caliper Life Sciences, Mountain View, CA) to detect flash-red fluorescence. Extensive PBS wash was performed to remove any cells adherent to the epicardium. Excitation was set at 640 nm and emission was set at 680 nm. Exposure time was set at 5 seconds and maintained the same during each imaging experiment. Fluorescence signals (photon/s) from a fixed region of interest (ROI) were measured and quantified with the Xenogen software. Organs from the CDC group (animals receiving non-labeled CDCs) were used as controls for background noise.

Quantification of engraftment by real time PCR

Quantitative PCR was performed 24 hr and 3 weeks after cell injection in 6 animals from each cell-injected group to quantify cell retention/engraftment. We injected CDCs from male donor WK rats into the myocardium of female recipients to utilize the detection of SRY gene located on the Y chromosome as target. The whole heart was harvested, weighed, and homogenized. Genomic DNA was isolated from aliquots of the homogenate corresponding to 12.5mg of myocardial tissue, using commercial kits (DNA Easy minikit, Qiagen). The TaqMan® assay (Applied Biosystems, CA) was used to quantify the number of transplanted cells with the rat SRY gene as template (forward primer: 5'-GGA GAG AGG CAC AAG TTG GC-3', reverse primer: 5'-TCC CAG CTG CTT GCT GAT C-3', TaqMan probe: 6FAM CAA CAG AAT CCC AGC ATG CAG AAT TCA G TAMRA, Applied Biosystems). A standard curve was generated with multiple dilutions of genomic DNA isolated from male hearts to quantify the absolute gene copy numbers. All samples were spiked with equal amounts of female genomic DNA as control. The copy number of the SRY gene at each point of the standard curve is

calculated with the amount of DNA in each sample and the mass of the rat genome per cell. For each reaction, 50 ng of template DNA was used. Real time PCR was performed with an Applied Biosystems 7900 HT Fast real-time PCR System. All experiments were performed in triplicate. The number of engrafted cells per heart was quantified by calculating the copy number of SRY gene in the total amount of DNA corresponding to 12.5 mg of myocardium and then extrapolating to the total weight of each heart.

Morphometric heart analysis

For morphometric analysis, 5-6 animals in each group were euthanized at 3 weeks and the hearts were harvested and frozen in OCT compound. Sections every 100 μm (10 μm thickness) were prepared. Masson's trichrome staining was performed as previously described[1]. Images were acquired with a PathScan Enabler IV slide scanner (Advanced Imaging Concepts, Princeton, NJ). From the Masson's trichrome-stained images, morphometric parameters including LV cavity circumference, total LV circumference, risk region area, scar area, non-infarcted region wall thickness and infarct wall thickness were measured in each section with NIH ImageJ software. To quantify both the degree of LV dilation and the degree of infarct wall thinning, the LV expansion index was calculated as previously described[2, 3]: LV Expansion index = (LV cavity circumference /total LV circumference) x (non-infarcted region wall thickness/risk region wall thickness). The percentage of viable myocardium as a fraction of the risk region was quantified as described[3].

Histology

For histology analysis, a subpopulation of animals in each group received Fe-CDCs or CDCs over-expressing GFP. At 24 hours or 3 weeks, the animals were euthanized and the hearts were harvested and frozen in OCT compound. Sections every 100 μm of the infarct and infarct border zone area (10 μm thickness) were prepared and immunocytochemistry for GFP and CD-68 (macrophages) was performed, using a rabbit anti-GFP (Abcam, Cambridge, MA, USA) and a Mouse anti rat CD68 (Abcam, Cambridge, MA, USA) primary antibody respectively. At the 3 week time point, immunocytochemistry for cardiomyocytes and endothelial cells were performed using a mouse anti-alpha-sarcomeric actin (Sigma) and rabbit anti-von Willebrand factor (Abcam) primary antibody respectively. Images were taken by a Leica TCS SP5 X confocal microscopy system.

Online Figures and Figure Legends

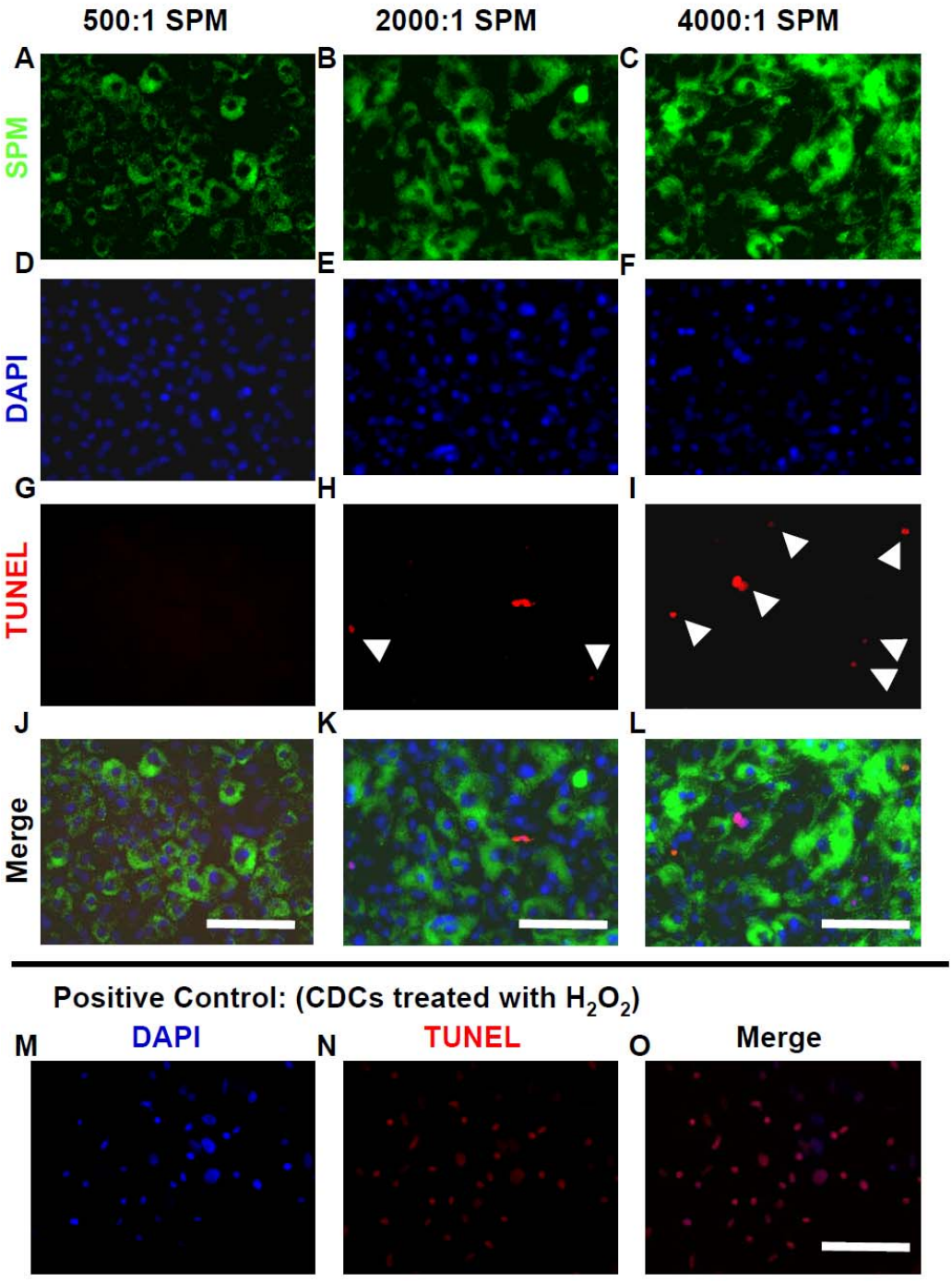

Online Figure I. Effects of SPM labeling on cell death. CDCs were co-incubated with SPMs for 24 hours at varying SPM:cell ratios: 500:1 (A, D, G, J); 2000:1 (B, E, H, K); 4000:1 (C, F, I, L). Apoptotic cells (red color) are highlighted by white arrowheads. M-O, images from positive controls (CDCs treated with H_2O_2). Bars = 50 μm.

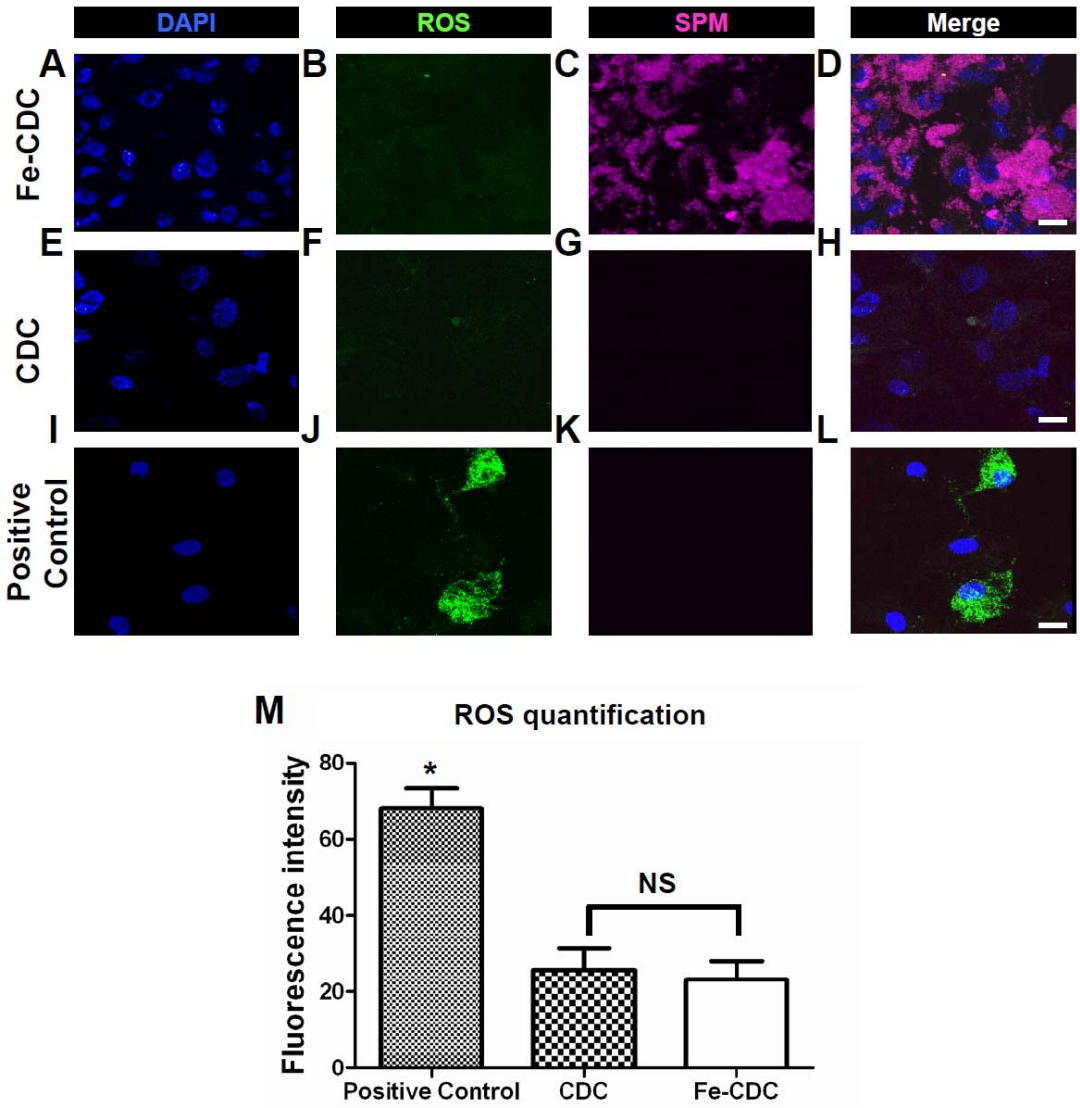

Online Figure II. Effects of SPM labeling on Reactive oxygen species (ROS) generation. A-D, Fe-CDCs: CDCs were co-incubated with SPMs for 24 hours at 500:1 SPM particle:cell ratio. E-H, plain CDCs. I-L, positive control: CDCs were treated with 100 μM H_2O_2 for 24 hours. ROS staining was detected by confocal microscopy imaging using the Image-iT™ LIVE Green Reactive Oxygen Species Detection Kit. M, Quantitative ROS measurement was performed by incubating cells with 6-carboxy-2',7'-dichlorodihydrofluorescein diacetate di(acetoxymethyl ester) (Invitrogen) for 60 min at a concentration of 10 μM. After that the fluorescence intensity was measured by a SpectraMax M5 plate reader. The ROS fluorescence intensities from the CDC and Fe-CDC group are indistinguishable, suggesting SPM labeling were not likely to elevate ROS generation. Bars = 10 μm. * indicates $P < 0.05$ when compared to the CDC or Fe-CDC group.

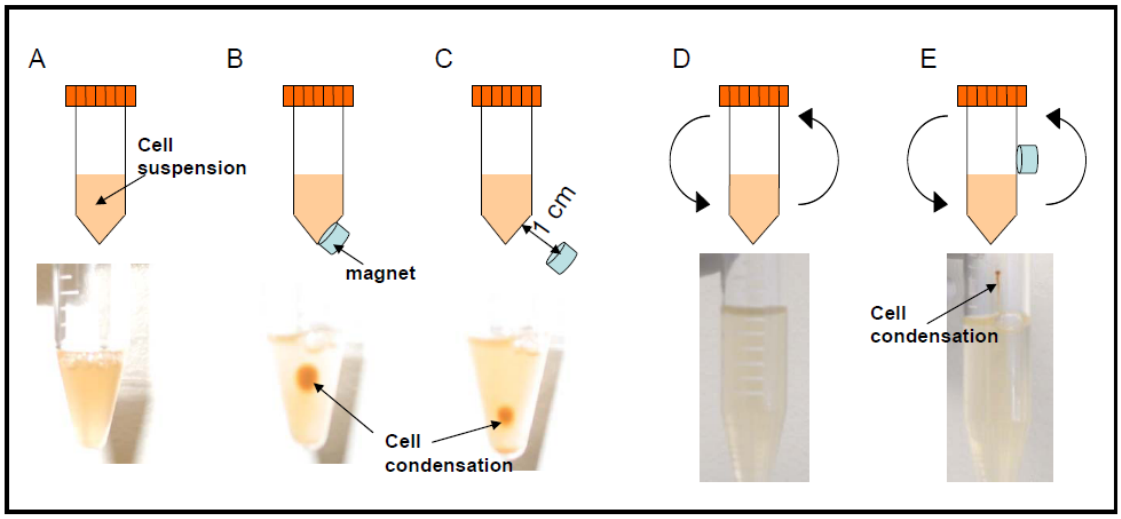

Online Figure III. Capturing of Fe-CDCs by magnet *in vitro*. A, Fe-CDCs were suspended in PBS (1 million cells/mL) in a 15 mL conical tube. Uniform cell suspension was obtained. B, cell condensate rapidly formed on the inner tube wall when a 1.3 Tesla magnet was placed on the outer tube wall for 20 seconds. C, a smaller cell condensate was formed when the same magnet was moved 1 centimeter away from the tube. D, without a magnet mounted on the tube, uniform cell suspension was obtained when the conical tube was rotated for 24 hours at 60 RPM. E, cell condensate was formed when the magnet was mounted on the tube during the rotation.

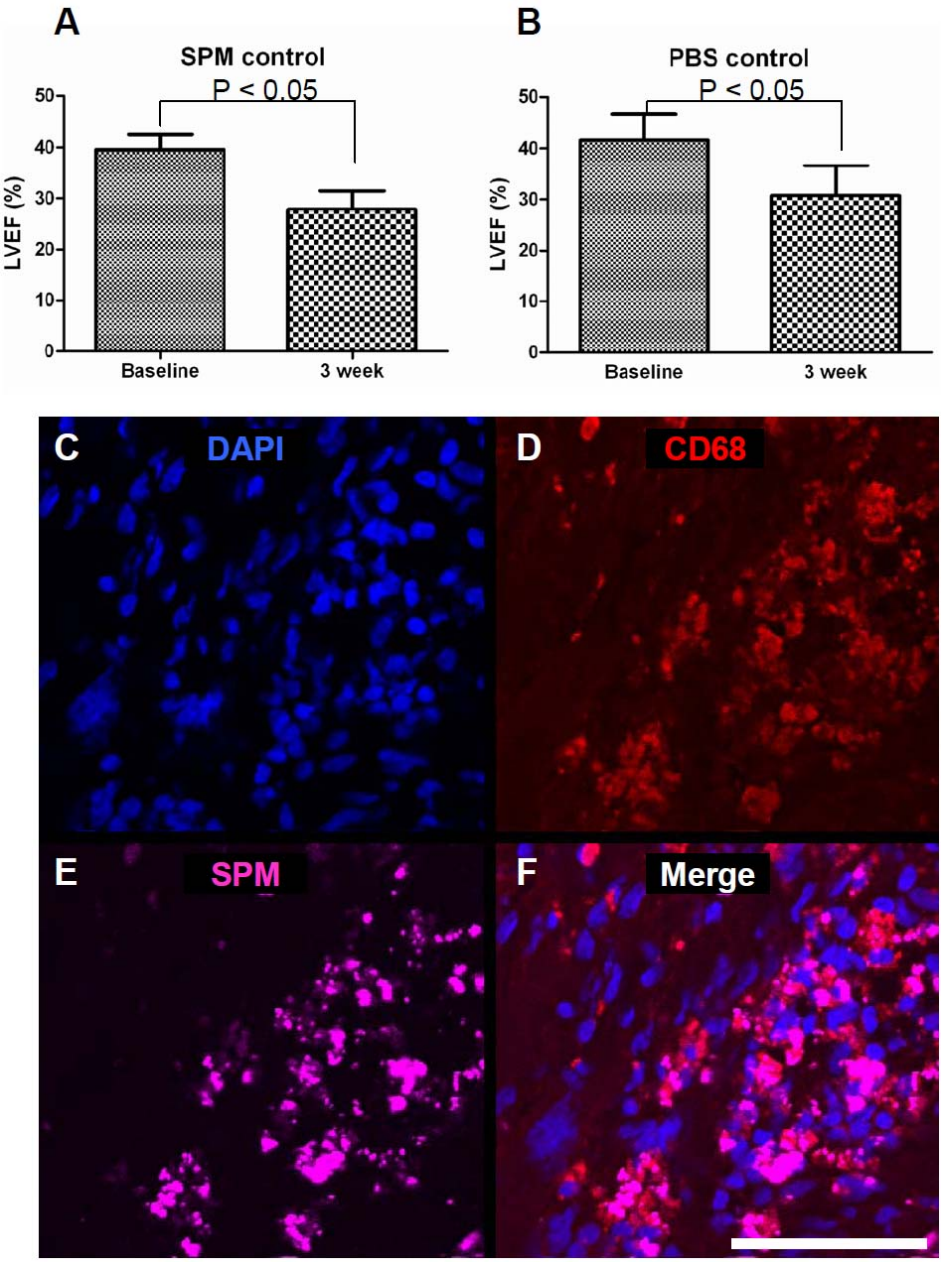

Online Figure IV. Injection of SPMs alone does not improve heart function. A, left ventricular ejection fraction (LVEF) measured by echocardiography at baseline and 3 weeks after injection of 500 million SPM beads in 100 µL PBS (n=9). B, LVEFs of PBS-injected animals (n=9; data reproduced from Figure 6). The effect of the SPM injection resembled that of PBS injection, as the LVEF decreased over time. This indicates that injection of SPMs alone did not have therapeutic benefits. C-F, immunohistochemistry staining of sections from SPM-injected hearts at 3 weeks. SPMs were present in the myocardium, with a large amount taken up by macrophages. Bar = 100 µm.

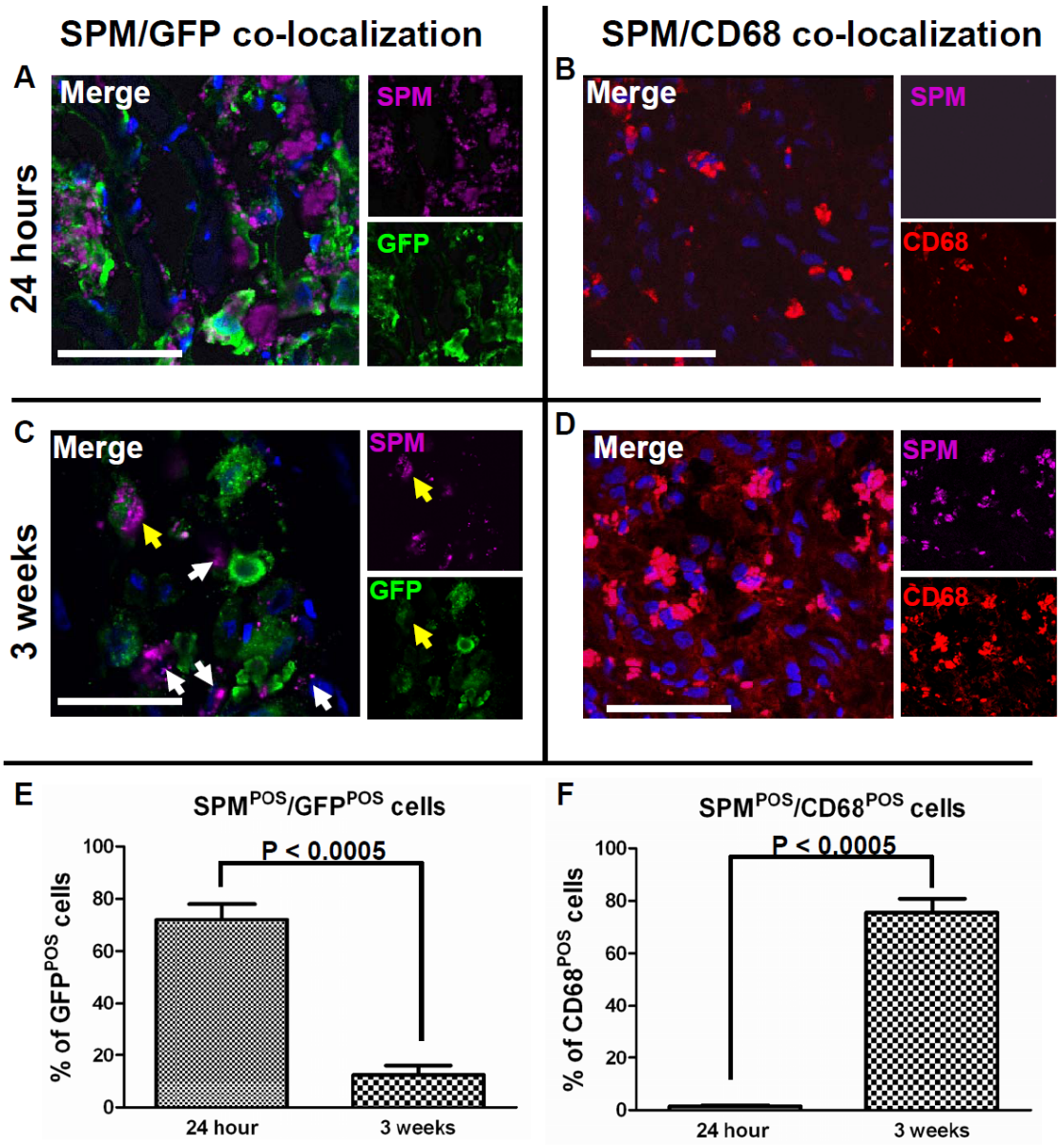

Online Figure V. Colocalization of SPM, GFP and CD-68. Subpopulations of animals from the Fe-CDC+Magnet group were euthanized at 24 hours and 3 weeks after injection. At the 24 hour time point, the majority of transplanted CDCs (GFP; green) were SPM positive (Flash red; magenta) (A). In contrast, the SPMs present in CD-68-positive macrophages (Texas red; red) were negligible (B). At the 3 week time point, only very few CDCs (C; yellow arrow) still contained SPMs. SPMs were found outside of the GFP-positive cells (C; white arrows). CD-68 staining confirmed the presence of macrophages and the majority of them were SPM positive (D). E & F, quantification of SPM/GFP and SPM/CD-68 colocalization at 24 hours and 3 weeks after cell injection. Bars = 50 µm.

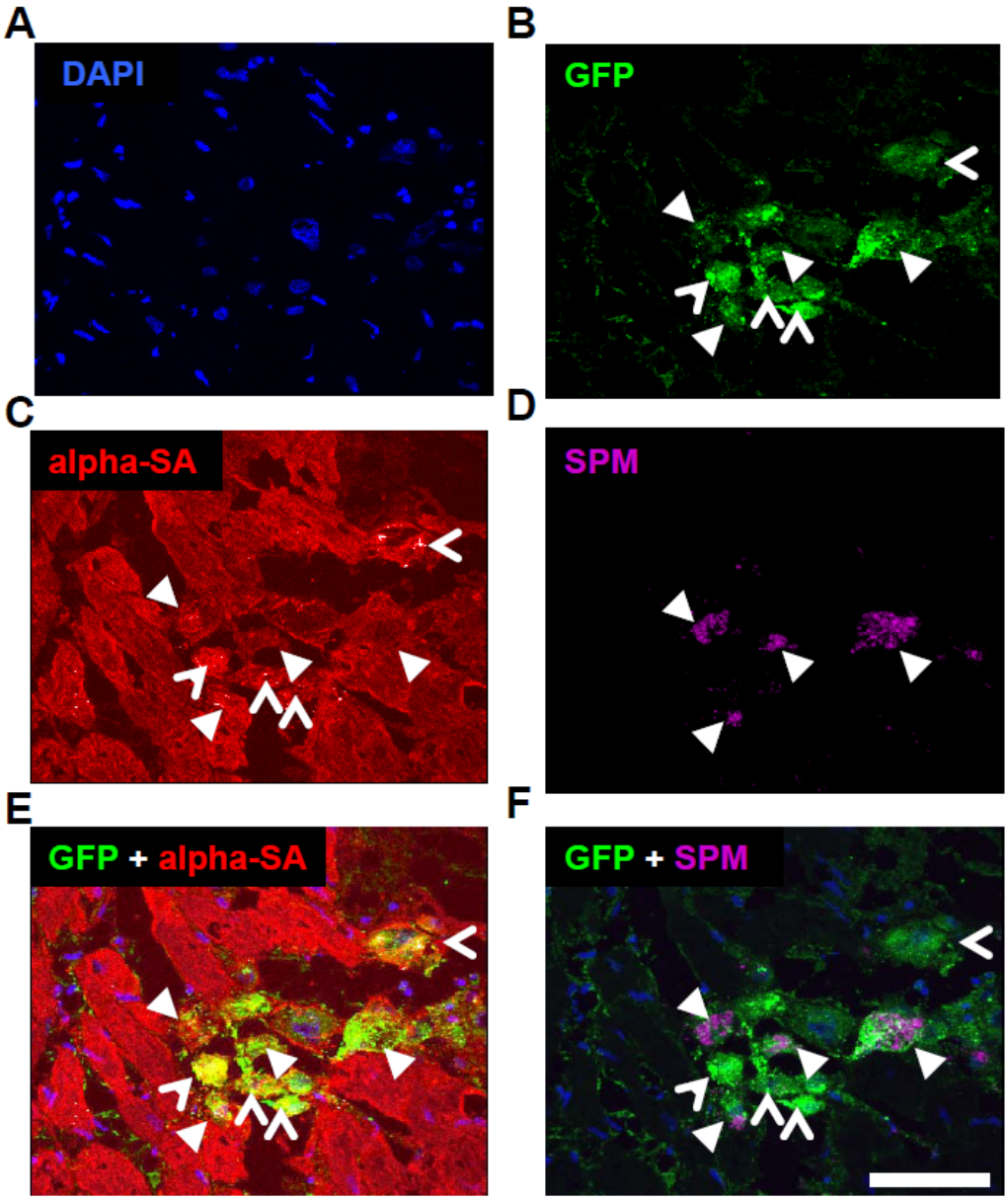

Online Figure VI. Expression of cardiac marker in SPM^{POS}/GFP^{POS} cells. Representative confocal images showing colocalization of GFP with alpha-sarcomeric actin (alpha-SA) in the peri-infarct region of a Fe-CDC+Magnet animal. A, DAPI; B, GFP; C, alpha-SA; D, SPM; E, GFP + alpha-SA; F, GFP + SPM. $SPM^{POS}/GFP^{POS}/alpha\text{-}SA^{POS}$ cells (solid white arrowheads "►") were detected in the region, indicating that remnant SPMs in the cytoplasm did not prevent CDCs from differentiating into a cardiomyocyte phenotype. $SPM^{NEG}/GFP^{POS}/alpha\text{-}SA^{POS}$ cells were also detected (empty white arrowheads ">"), indicative of cells that exocytosed the SPMs before or after acquiring a cardiomyocyte phenotype. Bars = 50 µm.

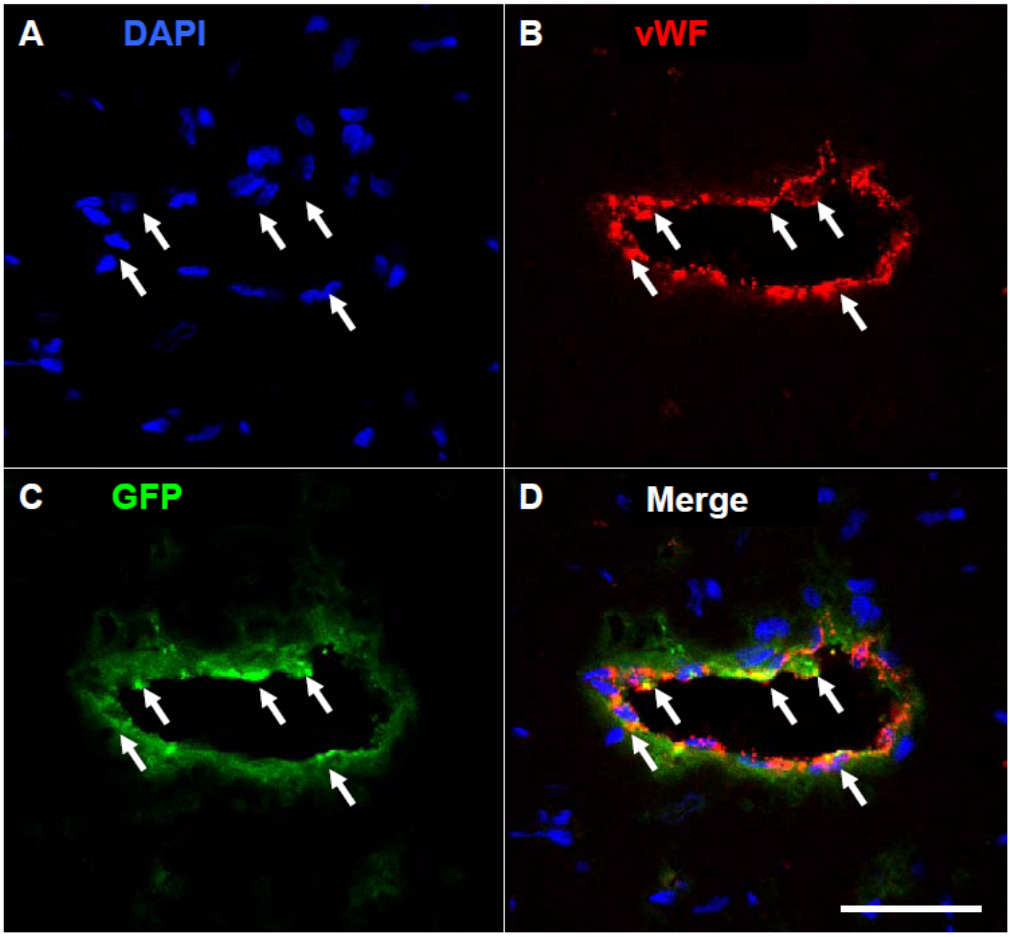

Online Figure VII. Expression of endothelial proteins in GFP^{POS} cells. Representative confocal images showing colocalization of GFP with von Willebrand factor (vWF) in an arteriole in the peri-infarct region of a Fe-CDC+Magnet animal. A, DAPI; B, vWF; C, GFP; D, merge. GFP^{POS}/vWF^{POS} cells are indicated by white arrows. The colocalization of GFP with vWF suggests that transplanted CDCs participated in regeneration of vascular structures, differentiating into an endothelial phenotype. Bars = 50 μm.

Online Table

Cell retention rate (%)	Time point	Cell type	Delivery method	Study model	References
11.1	10 min	Microspheres	IM	pig	[4]
17.6	1 hr	CDCs	IM	rat	[5]
5.5	1 hr	CD34+ cells	IC	human	[6]
11	1 hr	PMNCs	IM	pig	[7]
2.6	1 hr	PMNCs	IC	pig	[7]
3.2	1 hr	PMNCs	RCV	pig	[7]
1.3-2.6	75 min	BM stem cells	IC	human	[8]
2.03	24 hr	EPCs	IV	rat	[9]
4.70	24 hr	EPCs	ILV	rat	[9]
< 1	24 hr	CDCs	IC	pig	[10]
8	24 hr	CDCs	IM	pig	[11]

Online Table I. Survey of short-term cell retention. Short-term cell retention rates from several recent studies are summarized here. IM=intramyocardial, IC=intracoronary, RCV=retrograde coronary venous, IV=intravenous, ILV=intra LV cavity.

Supplemental References:

1. Smith RR, Barile L, Cho HC, Leppo MK, Hare JM, Messina E, Giacomello A, Abraham MR, Marban E. Regenerative Potential of Cardiosphere-Derived Cells Expanded From Percutaneous Endomyocardial Biopsy Specimens. *Circulation.* 2007;115:896-908.

2. Hochman JS, Choo H. Limitation of myocardial infarct expansion by reperfusion independent of myocardial salvage. *Circulation.* 1987;75:299-306.

3. Tang X-L, Rokosh G, Sanganalmath SK, Yuan F, Sato H, Mu J, Dai S, Li C, Chen N, Peng Y, Dawn B, Hunt G, Leri A, Kajstura J, Tiwari S, Shirk G, Anversa P, Bolli R. Intracoronary Administration of Cardiac Progenitor Cells Alleviates Left Ventricular Dysfunction in Rats With a 30-Day-Old Infarction. *Circulation.*121:293-305.

4. Teng CJ, Luo J, Chiu RCJ, Shum-Tim D. Massive mechanical loss of microspheres with direct intramyocardial injection in the beating heart: Implications for cellular cardiomyoplasty. *The Journal of Thoracic and Cardiovascular Surgery.* 2006;132:628-632.

5. Terrovitis J, Bonios M, Fox J, Engles JM, Yu J, Leppo MK, Pomper MG, Wahl RL, Seidel J, Tsui BM, Bengel FM, Abraham R, Marban E. Noninvasive Quantification and Optimization of Acute Cell Retention by In Vivo Positron Emission Tomography After Intramyocardial Cardiac-Derived Stem Cell Delivery. *Journal of the American College of Cardiology.* 2009;54:1619-1626.

6. Didier B, Michel T, Guy B, Micheline L, Philippe U, Nicolas P, Eric S, Dominique E, Jean-Paul D, Michel G, Serge G. Myocardial Homing of Nonmobilized Peripheral-Blood CD34+ Cells After Intracoronary Injection. *Stem Cells.* 2006;24:333-336.

7. Hou D, Youssef EA-S, Brinton TJ, Zhang P, Rogers P, Price ET, Yeung AC, Johnstone BH, Yock PG, March KL. Radiolabeled Cell Distribution After Intramyocardial, Intracoronary, and Interstitial Retrograde Coronary Venous Delivery: Implications for Current Clinical Trials. *Circulation.* 2005;112:I-150-156.

8. Hofmann M, Wollert KC, Meyer GP, Menke A, Arseniev L, Hertenstein B, Ganser A, Knapp WH, Drexler H. Monitoring of Bone Marrow Cell Homing Into the Infarcted Human Myocardium. *Circulation.* 2005;111:2198-2202.

9. Aicher A, Brenner W, Zuhayra M, Badorff C, Massoudi S, Assmus B, Eckey T, Henze E, Zeiher AM, Dimmeler S. Assessment of the Tissue Distribution of Transplanted Human Endothelial Progenitor Cells by Radioactive Labeling. *Circulation.* 2003;107:2134-2139.

10. Johnston PV, Sasano T, Mills K, Evers R, Lee S-T, Smith RR, Lardo AC, Lai S, Steenbergen C, Gerstenblith G, Lange R, Marban E. Engraftment, Differentiation, and Functional Benefits of Autologous Cardiosphere-Derived Cells in Porcine Ischemic Cardiomyopathy. *Circulation.* 2009;120:1075-1083.

11. Lee S-T, White AJ, Matsushita S, Li T-S, Malliaras K, Chowdhury S, Glenn A, Zeng H, Zhang Y, Terrovitis I, Simsir S, Makkar R, Marban E. Abstract 3976: Direct Intramyocardial Injection of Autologous Cardiosphere-Derived Cells

Yields Consistent Engraftment and Improves Cardiac Function in a Porcine Model of Ischemic Cardiomyopathy. *Circulation.* 2009;120:S898-b-.

Legends for the Supplemental Video Files

Online Movie I. Representative video capturing cell injection procedure without magnetic targeting (Fe-CDC). The yellow-brown cells wash out quickly after injection.

Online Movie II. Representative video capturing cell injection procedure with magnetic targeting (Fe-CDC + Magnet). The yellow-brown cells are drawn towards the apex and persist in the heart after injection.